

DE-BIASING PARTICLE FILTERING FOR A CONTINUOUS TIME HIDDEN MARKOV MODEL WITH A COX PROCESS OBSERVATION MODEL

RUIYANG JIN, SUMEETPAL S. SINGH, AND NICOLAS CHOPIN

ABSTRACT. We develop a (nearly) unbiased particle filtering algorithm for a specific class of continuous-time state-space models, such that (a) the latent process X_t is a linear Gaussian diffusion; and (b) the observations arise from a Poisson process with intensity $\lambda(X_t)$. The likelihood of the posterior probability density function of the latent process includes an intractable path integral. Our algorithm relies on Poisson estimates which approximate unbiasedly this integral. We show how we can tune these Poisson estimates to ensure that, with large probability, all but a few of the estimates generated by the algorithm are positive. Then replacing the negative estimates by zero leads to a much smaller bias than what would obtain through discretisation. We quantify the probability of negative estimates for certain special cases and show that our particle filter is effectively unbiased. We apply our method to a challenging 3D single molecule tracking example with a Born and Wolf observation model.

1. INTRODUCTION

1.1. Background. Diffusion processes have been extensively used for modelling continuous-time phenomena in a range of scientific areas, including finance [4, 22], biochemistry [15, 16, 21], physics [26] and engineering [28]. These processes are usually applied to model both the observed process and an unobserved signal/state process in a hierarchical model.

This paper develops novel methods for optimal filtering of multivariate diffusion processes observed at irregular time instances, which follow a Cox process whose intensity is a (non-negative) function of the state process. The complete data likelihood of such a model includes a path integral of the state trajectory (through the intensity function), which is intractable. This precludes the use of standard particle filters.

Another common recognised problem in continuous time filtering for diffusion processes is the unavailability of transition densities [13, 18]. In our problem though, the hidden state is described by a linear SDE and thus state transition density is available, but the likelihood still remains intractable for the reason mentioned above. Estimators proposed by [24] replaces the path integral (with respect to time) with a Riemann approximation based on a number of intermediate points. This technique is further used to construct the transition density estimator of [10] and implemented in filtering context to approximate the weights.

To remove the time-discretisation error in the numerical approximation of the path integral, the so-called Poisson estimator is often deployed. The path integral estimate is computed using a (infinite) series expansion which is expressed as a random finite series

(RJ) DEPARTMENT OF ENGINEERING, UNIVERSITY OF CAMBRIDGE

(SSS) DEPARTMENT OF ENGINEERING, UNIVERSITY OF CAMBRIDGE

(NC) ENSAE, INSTITUT POLYTECHNIQUE DE PARIS

Key words and phrases. Sequential Monte Carlo; Particle filter; Diffusions; Continuous-time; Hidden Markov model; Cox process; Path integral; Poisson estimate.

where the random truncation is given by a Poisson random variable. The first Poisson estimator was introduced in the field of statistical physics by [32, 33]. This was subsequently further developed in the computational statistics literature, to provide an unbiased estimation of diffusion transition densities by [3], to its generalisation forms and its use in sequential importance sampling by [12], and to its variant using power series expansion by [27]. One drawback of using a Poisson estimator is that it may return negative values, which can result in an overall negative likelihood estimate and thus prohibiting the use of the likelihood estimate for model calibration via Particle MCMC [1]. A naive way to ensure positive estimates is to truncate all negative estimates to zero, which obviously comes at the expense of introducing a bias to the estimate. [13] use Wald’s identity (for martingales) to generate an unbiased estimate of the path integral that are guaranteed to be positive. However, this method does not seem to yield an unbiased estimate of the likelihood itself (see Section 4.1.3 for an elaboration on this point), and has a bias which appears difficult to quantify.

1.2. Contributions. The approach we pursue in this work is to employ the standard Poisson estimate and retain only the positive part of the returned estimate. (In Section 4.1.3, we discuss the retaining the absolute value which will allow us to completely de-bias the estimate.) We are able to quantify the probability of encountering a negative weight (in certain idealised scenarios) and show that this probability decreases exponentially with the inverse of the time interval size over which the estimate is computed. (For some typical experimental settings in our numerical work the probability is exceptionally small, of the order 10^{-50} .) This exponential decrease in the probability of a negative estimate yields a few extra boons. The first being a rapidly diminishing mean square error, for the likelihood estimate, in the available CPU time. The second being the probability a complete run of an N -particle approximation for T/Δ time steps encountering a negative estimate (thus needing truncation) being equally rare and straightforward to control using our proposed (heuristic) tuning procedure. (Here $[0, T]$ is the time interval for smoothing, Δ is the interval over which the path integral is estimated and thus there are T/Δ path integrals to estimate for each particle.) To control a negative weight event, the extra simulation cost per-particle per-time step is $\mathcal{O}(\Delta)$ and thus the total extra cost is $N \times (T/\Delta) \times \Delta$, which does not blow up Δ tends to zero.

As for our second contribution, we apply our methodology to a challenging model calibration problem arising from single molecule fluorescence microscopy, which is a very popular live cell imaging technology. We combine our likelihood estimate with the particle marginal Metropolis-Hastings algorithm [1] to estimate the model parameters for data that arises from observing a diffusing molecule in 3D via a Cox process and a Born-Wolf observation model. We show how our particle filter significantly outperforms the conventional time discretisation based approach for the intractable path integral as implemented in [8]. Our method is shown to have a negligible bias due to our tuning heuristic that controls the occurrence of a negative Poisson path integral estimate (and thus the truncation induced bias).

The paper is organised as follows. Section 2 presents the problem formulation while Sections 3 and 4 present the particle filtering methodology in continuous time. Section 3 presents the particle filter that employs a simple time discretisation of the path integral and Section 4 the more sophisticated particle filter that employs the Poisson estimator of the path integral. Our proposed algorithm and accompanying theoretical results on its performance are also presented in Section 4. Experiments including likelihood estimation,

state estimation (smoothing) and parameter estimation are presented in Section 5. Proofs and additional algorithms can be found in the Appendix.

2. PROBLEM FORMULATION

2.1. Notation. We consider a latent continuous time Markov process $\{X_t\}_{t \geq 0}$ which takes values in $\mathcal{X} \subset \mathbb{R}^n$, has a time-inhomogeneous Markov transition density, $X_{t_k} | (X_{t_{k-1}} = x_{k-1}) \sim f_{t_{k-1}, t_k}^\theta(x_k | x_{k-1})$, and initial density ν^θ . The superscript θ is the parameter of the model, and will be defined subsequently. By $X \sim \mathcal{N}(\mu, \Sigma)$, we mean that X has the distribution of a Gaussian random variable with mean μ and covariance Σ , whereas $\mathcal{N}(x; \mu, \Sigma)$ is the evaluation this Gaussian density at x . We use the standard sequence notation $i : j = i, i + 1, \dots, j - 1, j$, and $\lceil x \rceil$ to denote the smallest integer number greater than or equal to $x \in \mathbb{R}$. The $\mathcal{Y} \subset \mathbb{R}^m$ -valued stochastic process $\{Y_k\}_{k \in \mathbb{Z}_+}$ corresponds to the observed process with observation density $g^\theta(y_k | x_k)$. A realisation of a Poisson point process on the positive real line is a sequence of increasing time points $0 < t_1 < t_2 < \dots$ generated according to a non-negative intensity function $t \mapsto \lambda_t$. For our application, the intensity function is stochastic and state dependent, i.e. $\lambda_t = \lambda(X_t) \geq 0$.

2.2. Hidden Markov Model Formulation. Let $(t_1, y_{t_1}), \dots, (t_{n_p}, y_{t_{n_p}})$ be an observed sequence of non-negative increasing arrival times $0 < t_i < T$ and arrival locations y_{t_i} of a marked Poisson point process on the real line, recorded in the time interval $[0, T]$. The arrival times are generated by a Poisson point process on $[0, \infty)$ with stochastic intensity function $\lambda(X_t)$, which is determined by a latent continuous time Markov process $\{X_t\}_{t \geq 0} \subset \mathcal{X}$ and a non-negative real valued function $\lambda : \mathcal{X} \rightarrow \mathbb{R}$. The locations $y_{t_i} \in \mathcal{Y}$ are marks of the point process and are generated according to the conditional (on $X_{t_i} = x$) probability density function,

$$Y_{t_i} | (X_{t_i} = x) \sim g^\theta(y | x) dy, \quad i \in \{1 : n_p\}.$$

The *exact* likelihood is

$$(1) \quad \mathcal{L} = \mathbb{E} \left\{ \left(\prod_{i=1}^{n_p} \lambda(X_{t_i}) g^\theta(y_{t_i} | X_{t_i}) \right) \times \exp \left(- \int_0^T \lambda(X_s) ds \right) \right\}$$

where the expected value is computed with respect to the law of $\{X_t\}_{0 \leq t \leq T}$.

3. PARTICLE FILTERING

We adopt a discretisation of the positive real axis which is divided into segments of maximum length Δ defined sequentially as follows:

$$(2) \quad \begin{aligned} t_0^\Delta &= 0, \\ t_k^\Delta &= t_{k-1}^\Delta + \min \left\{ \Delta, T - t_{k-1}^\Delta, \min_{t_i > t_{k-1}^\Delta} t_i - t_{k-1}^\Delta \right\}, \quad k > 1 \end{aligned}$$

where t_i is the (observed) arrival time. Thus (2) defines an increasing sequence of time points $t_0^\Delta = 0 < t_1^\Delta < \dots < t_{m-1}^\Delta < t_m^\Delta = T$ spaced Δ apart unless the spacing is narrowed to coincide with the arrival of the observation y_{t_i} at time t_i and ensures $\{t_1, \dots, t_{n_p}\} \subset \{t_1^\Delta, \dots, t_{m-1}^\Delta\}$. The *exact* likelihood (1) may be re-expressed using time points t_i^Δ as

$$(3) \quad \mathcal{L} = \mathbb{E} \left\{ \left(\prod_{i=1}^{n_p} \lambda(X_{t_i}) g^\theta(y_{t_i} | X_{t_i}) \right) \times \left(\prod_{j=1}^m \exp \left(- \int_{t_{j-1}^\Delta}^{t_j^\Delta} \lambda(X_s) ds \right) \right) \right\}.$$

The exact likelihood is not straightforwardly (using an approach such as in Algorithm 1) amenable to unbiased estimation using particle filtering due to the path-integrals of $\lambda(X_s)$.

Algorithm 1: Bootstrap particle filter

```

1 for  $i \in \{1 : N\}$  do
2   Sample  $X_0^{(i)} \sim \nu^\theta(\cdot)$ .
3   Set  $W_0^{(i)} = \exp\left(-X_0^{(i)}(t_1^\Delta - t_0^\Delta)\right)$ .
4   Resample  $\{X_0^{(i)}, W_0^{(i)}\}$  to obtain  $\{\tilde{X}_0^{(i)}, \frac{1}{N}\}$ .
5 end
6 for  $k \in \{1 : m-1\}$  do
7   for  $i \in \{1 : N\}$  do
8     Sample  $X_k^{(i)} \sim f_{t_{k-1}^\Delta, t_k^\Delta}^\theta(\cdot | \tilde{X}_{k-1}^{(i)})$  and set  $X_{0:k}^{(i)} = (\tilde{X}_{0:k-1}^{(i)}, X_k^{(i)})$ .
9     Set
10      
$$W_k^{(i)} = \exp\left(-X_k^{(i)}(t_{k+1}^\Delta - t_k^\Delta)\right) \times \prod_{j=1}^{n_p} \left(\lambda(X_k^{(i)})g^\theta(y_{t_j} | X_k^{(i)})\right)^{\mathbb{I}[t_k^\Delta \leq t_j < t_{k+1}^\Delta]}.$$

11      % Find all  $y_{t_j}$  with  $t_j \in [t_k^\Delta, t_{k+1}^\Delta)$ .
12     Resample  $\{X_{0:k}^{(i)}, W_k^{(i)}\}$  to obtain  $\{\tilde{X}_{0:k}^{(i)}, \frac{1}{N}\}$ .
13   end
14 end

```

14 Compute the (unbiased) estimate of the likelihood in (4):

$$(6) \quad \hat{\mathcal{L}}_\Delta = \prod_{k=0}^{m-1} \left\{ \frac{1}{N} \sum_{i=1}^N W_k^{(i)} \right\}.$$

A simple approach is to replace the path-integral over $[0, T]$ with the following Reimann approximation

$$(4) \quad \mathcal{L}_\Delta = \mathbb{E} \left\{ \left(\prod_{i=1}^{n_p} \lambda(X_{t_i}) g^\theta(y_{t_i} | X_{t_i}) \right) \times \prod_{j=1}^m \exp\left(-\lambda(X_{t_{j-1}^\Delta})(t_j^\Delta - t_{j-1}^\Delta)\right) \right\}$$

(The subscript Δ denotes the dependence on the time discretisation and emphasises that $\mathcal{L}_\Delta \neq \mathcal{L}$.) The posterior density function of $(X_0, X_1, \dots, X_m) = (X_{t_0^\Delta}, X_{t_1^\Delta}, \dots, X_{t_m^\Delta})$ for this time discretised model is

$$(5) \quad \int p_\Delta^\theta(x_0, \dots, x_m) h(x_{0:m}) dx_{0:m} \\ \propto \mathbb{E} \left\{ h\left(X_{t_0^\Delta}, \dots, X_{t_m^\Delta}\right) \times \left(\prod_{i=1}^{n_p} \lambda(X_{t_i}) g^\theta(y_{t_i} | X_{t_i}) \right) \times \prod_{j=1}^m \exp\left(-\lambda(X_{t_{j-1}^\Delta})(t_j^\Delta - t_{j-1}^\Delta)\right) \right\}$$

This posterior density function and its likelihood can be estimated using a conventional particle filter as described in Algorithm 1 [8].

The estimate $\hat{\mathcal{L}}_\Delta$ returned by Algorithm 1 is an unbiased estimate of the time-discretised likelihood \mathcal{L}_Δ . In the next section we will develop a particle method that approximates the exact (not-discretised) likelihood, and in the numerical section (Section 5) we will extensively contrast its estimation accuracy compared to Algorithm 1 applied to model (5).

4. PARTICLE FILTERING TO MITIGATE MODEL DISCRETISATION ERROR

We propose a simple method to nearly unbiasedly estimate the true likelihood \mathcal{L} . The idea is to discretise the path integrals into smaller Δ length time integrals, $\exp\left(-\int_t^{t+\Delta}\lambda(X_s)ds\right)$, which are amenable to simple unbiased estimation and whose probability of being positive approaches 1 rapidly as Δ tends to 0. We truncate a negative estimate to 0, and when combined with the rarity of such events, it is simple to quantify the bias, which is also shown to be rapidly decreasing as Δ tends to 0. This estimate can be used within particle filtering and Particle MCMC; such methods are known as particle filtering with “random weights” as in [29], [12] and [13].

Specifically, we are going to construct real valued random variables E_1, \dots, E_m , which are conditionally independent given $X_{t_0^\Delta}, \dots, X_{t_m^\Delta}$ (in the manner made precise below in (7)) and each unbiasedly estimates the corresponding term $\exp(-\int_{t_{i-1}^\Delta}^{t_i^\Delta}\lambda(X_s)ds)$ in the manner of (8):

$$(7) \quad p(e_1, \dots, e_m | x_{t_0^\Delta}, \dots, x_{t_m^\Delta}) = \prod_{i=1}^m p_{t_{i-1}^\Delta, t_i^\Delta}(e_i | x_{t_{i-1}^\Delta}, x_{t_i^\Delta})$$

$$(8) \quad \int_{-\infty}^{\infty} e_i p_{t_{i-1}^\Delta, t_i^\Delta}(e_i | x_{t_{i-1}^\Delta}, x_{t_i^\Delta}) de_i = \mathbb{E}\left\{\exp\left(-\int_{t_{i-1}^\Delta}^{t_i^\Delta}\lambda(X_s)ds\right) \mid X_{t_{i-1}^\Delta} = x_{t_{i-1}^\Delta}, X_{t_i^\Delta} = x_{t_i^\Delta}\right\}.$$

With these random variables E_1, \dots, E_m , we retain the unbiasedness of the estimate of the numerator and denominator (the likelihood),

$$\begin{aligned} & \int p_T(x_{0:m}) h(x_{0:m}) dx_{0:m} \\ & \propto \mathbb{E}\left\{h(X_{t_0^\Delta}, X_{t_1^\Delta}, \dots, X_{t_m^\Delta}) \times \left(\prod_{i=1}^{n_p} \lambda(X_{t_i}) g^\theta(y_{t_i} | X_{t_i})\right) \times \prod_{j=1}^m E_j\right\} \end{aligned}$$

which follows through a conditioning expectation argument. For $k \in \{1 : m\}$, let

$$(9) \quad \begin{aligned} & \int p_{t_k^\Delta}(x_0, \dots, x_k) h_k(x_{0:k}) dx_{0:k} \\ & \propto \mathbb{E}\left\{h_k(X_{t_0^\Delta}, X_{t_1^\Delta}, \dots, X_{t_k^\Delta}) \times \left(\prod_{i=1}^{n_p} [\lambda(X_{t_i}) g^\theta(y_{t_i} | X_{t_i})]^{1_{[t_i \leq t_k^\Delta]}}\right) \times \prod_{j=1}^k E_j\right\} \end{aligned}$$

where, recall, $t_m = T$. Once we have defined (7), it will be straightforward to construct a particle approximation of the conditional probability density functions (9). These posterior densities, unlike (5), do not have a time discretisation bias. Our particle filtering algorithm, detailed in Algorithm 3, also returns an estimate of the exact likelihood (3).

The next subsection explains how to construct these variables E_i using the Poisson estimate approach. The following subsections will explain how to ensure that the probability of $E_i < 0$ may be made negligible.

4.0.1. *The Poisson Estimator.* We first consider a fixed trajectory $\{X_s\}_{0 < s \leq t_1^\Delta}$, then

$$\begin{aligned}
\exp\left(-\int_0^{t_1^\Delta} \lambda(X_s) ds\right) &= \exp(c) \exp(I - c) \\
&= \exp(c) \sum_{k=0}^{\infty} \frac{(I - c)^k}{k!} \\
&= \exp(c + \eta) \sum_{k=0}^{\infty} \exp(-\eta) \frac{\eta^k}{k!} \left(\frac{I - c}{\eta}\right)^k \\
&= \exp(c + \eta) \sum_{k=0}^{\infty} \exp(-\eta) \frac{\eta^k}{k!} \prod_{i=1}^k \mathbb{E}_{\tau_i} \left(\frac{-t_1^\Delta \lambda(X_{\tau_i}) - c}{\eta}\right) \\
&= \exp(c + \eta) \mathbb{E}_\kappa \left[\prod_{i=1}^{\kappa} \mathbb{E}_{\tau_i} \left(\frac{-t_1^\Delta \lambda(X_{\tau_i}) - c}{\eta}\right) \right],
\end{aligned}$$

where $I = -\int_0^{t_1^\Delta} \lambda(X_s) ds$ and $-t_1^\Delta \lambda(X_{\tau_i})$'s are the unbiased estimates of I . The above derivation follows the approach outlined in [27].

The inclusion of constant c is to optimise the resulting estimator. The inclusion of $\mathcal{P}o(\eta)$ distribution is to allow an unbiased estimate to be based on a truncated sum and finally $\mathbb{E}_\kappa(\cdot)$ and $\mathbb{E}_{\tau_i}(\cdot)$ denote expectation with respect to $\kappa \sim \mathcal{P}o(\eta)$ and $\tau_i \sim \mathcal{U}(0, t_1^\Delta)$. The final line yields the resulting unbiased estimator:

$$(10) \quad E_1 = \exp(c + \eta) \left[\mathbb{I}_{\{\kappa=0\}} + \mathbb{I}_{\{\kappa>0\}} \left(\prod_{i=1}^{\kappa} \frac{-t_1^\Delta \lambda(X_{\tau_i}) - c}{\eta} \right) \right]$$

as the sample from $E_1 \sim p(e_1 | x_0, x_{t_1^\Delta})$.

[27] discussed how to choose c and η in order to make the variance of the estimate as small as possible. In particular, he showed that $c^* = I - \eta$ is the value of c that minimises the variance (for a fixed η). Our approach is slightly different: we aim at controlling the probability of the estimate being negative. For that purpose, we set $c = -t_1^\Delta \lambda(X_0) - \eta$ (which can also be seen as a tractable approximation of c^*). This yields:

$$E_1 = \exp\{-t_1^\Delta \lambda(X_0)\} \left[\mathbb{I}_{\{\kappa=0\}} + \mathbb{I}_{\{\kappa>0\}} \left(\prod_{i=1}^{\kappa} \left[1 + \frac{t_1^\Delta}{\eta} (\lambda(X_0) - \lambda(X_{\tau_i})) \right] \right) \right].$$

We postpone the discussion on how to control the probability of a negative estimate to the next sub-section.

The Poisson estimator for any time interval $t_{i-1}^\Delta \leq t \leq t_i^\Delta$ is detailed in Algorithm 2. Note that we assume we can exactly sample X_{τ_j} from $p(x_\tau | x_{\tau_{j-1}})$ for $j \in \{1 : \kappa\}$. This is possible for linear Gaussian diffusions, as discussed in the introduction; see Appendix A for details.

The particle filter with the Poisson estimator is described in Algorithm 3. Step 8 of this algorithm makes a call to Algorithm 2 to get the desired samples $E_k^{(i)}$ from $p(e_k | X_{t_{k-1}^\Delta}^{(i)}, X_{t_k^\Delta}^{(i)})$.

4.1. Negative Poisson Estimate Control. Although the Poisson estimator can return negative values, the following lemma shows that the probability of this happening is controllable by adjusting (η, Δ) and in particular decays exponentially fast in Δ .

Algorithm 2: $\text{PE}(\eta, t_{i-1}^\Delta, t_i^\Delta, X_{t_{i-1}^\Delta})$

Input: $\eta, t_{i-1}^\Delta, t_i^\Delta, X_{t_{i-1}^\Delta}$

- 1 Generate $\kappa \sim \mathcal{P}o(\eta)$.
- 2 Generate $\tau_1, \tau_2, \dots, \tau_\kappa \sim \mathcal{U}(t_{i-1}^\Delta, t_i^\Delta)$, sort them in ascending order and relabel them so that $\tau_1 < \tau_2 < \dots < \tau_\kappa$.
- 3 Sequentially sample X_{τ_j} from $p(x_\tau | x_{\tau_{j-1}})$ for $j \in \{1 : \kappa\}$ where $\tau_0 = t_{i-1}^\Delta$. Sample $X_{t_i^\Delta}$ from $p(x_{t_i^\Delta} | x_{\tau_\kappa})$.
- 4 Compute and return the estimate:

$$E = \exp\left(- (t_i^\Delta - t_{i-1}^\Delta) \times \lambda\left(X_{t_{i-1}^\Delta}\right)\right) \times \left[\mathbb{I}_{\{\kappa=0\}} + \mathbb{I}_{\{\kappa>0\}} \left(\prod_{j=1}^{\kappa} \left[1 + \frac{t_i^\Delta - t_{i-1}^\Delta}{\eta} \left(\lambda(X_{t_{i-1}^\Delta}) - \lambda(X_{\tau_j}) \right) \right] \right) \right].$$

Output: $(E, X_{t_i^\Delta})$ % The sample from $p(e, x_{t_i^\Delta} | X_{t_{i-1}^\Delta})$

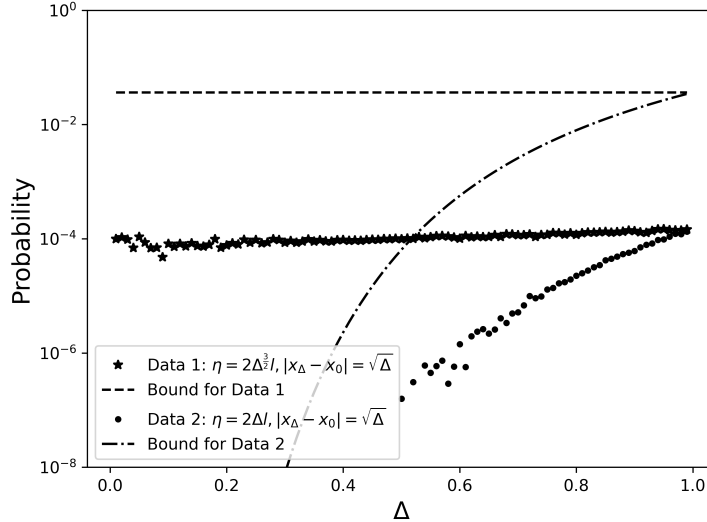
Algorithm 3: Bootstrap particle filter in continuous time

- 1 Find Δ (15) and define time steps (2).
- 2 **for** $i \in \{1 : N\}$ **do**
- 3 Sample $\tilde{X}_{t_0^\Delta}^{(i)} \sim \nu^\theta(\cdot)$ and set $W_0^{(i)} = \frac{1}{N}$.
- 4 Estimate \hat{l}_0 . % See Section 4.1.1.
- 5 **for** $k \in \{1 : m\}$ **do**
- 6 **for** $i \in \{1 : N\}$ **do**
- 7 Set $\eta_k = (t_k^\Delta - t_{k-1}^\Delta) \hat{l}_{k-1}$.
- 8 Sample $(E_k^{(i)}, X_{t_k^\Delta}^{(i)}) \leftarrow \text{PE}(\eta_k, t_{k-1}^\Delta, t_k^\Delta, \tilde{X}_{t_{k-1}^\Delta}^{(i)})$ and set $(X_{t_0^\Delta}^{(i)}, \dots, X_{t_k^\Delta}^{(i)}) = (\tilde{X}_{t_0^\Delta}^{(i)}, \dots, \tilde{X}_{t_{k-1}^\Delta}^{(i)}, X_{t_k^\Delta}^{(i)})$.
- 9 Update \hat{l}_k using (16).
- 10 Set $W_k^{(i)} = \max\{E_k^{(i)}, 0\} \times \prod_{j=1}^{n_p} \left(\lambda(\tilde{X}_{t_{k-1}^\Delta}^{(i)}) g^\theta(y_{t_j} | \tilde{X}_{t_{k-1}^\Delta}^{(i)}) \right)^{\mathbb{I}[t_j=t_{k-1}^\Delta]}$.
- 11 % Incorporating y_{t_j} with $t_j = t_{k-1}^\Delta$.
- 12 Resample $\{(X_{t_0^\Delta}^{(i)}, \dots, X_{t_k^\Delta}^{(i)}), W_k^{(i)}\}$ to obtain $\{(\tilde{X}_{t_0^\Delta}^{(i)}, \dots, \tilde{X}_{t_k^\Delta}^{(i)}), \frac{1}{N}\}$.
- 13 Compute the likelihood estimate:

$$(11) \quad \hat{\mathcal{L}} = \prod_{k=1}^m \left\{ \frac{1}{N} \sum_{i=1}^N W_k^{(i)} \right\}.$$

Lemma 1. Let $\{X_s\}_{0 \leq s \leq \Delta}$ be one dimensional Brownian motion which starts at $X_0 = x_0$. Consider the estimate (10) (with $t_1^\Delta = \Delta$) of the path integral $\mathbb{E} \left\{ \exp\left(- \int_0^\Delta \lambda(X_s) ds\right) \middle| X_\Delta = x_\Delta \right\}$. Let $\lambda(\cdot)$ be a non-negative l -Lipschitz function, then the following bound holds when $\eta > \Delta l |x_\Delta - x_0|$,

$$(12) \quad \Pr\left(E_1 < 0 | \kappa > 0, X_\Delta = x_\Delta\right) < 2 \exp\left\{ - \frac{2\eta}{\Delta l} \left(\frac{\eta}{\Delta l} - |x_\Delta - x_0| \right) \right\}.$$

FIGURE 1. Plot of probability (12) vs. Δ for different choices of η .

Proof. See Appendix B. □

Note that the estimate is trivially positive when $\kappa = 0$ and hence the bound is given conditionally on $\kappa > 0$. An illustration of how $\Pr(E_1 < 0 | \kappa > 0)$ and its corresponding bound evolve as Δ changes for different choices of η is provided in Figure 1. Each data point is a Monte Carlo estimate of the conditional probability (conditioned on $\kappa > 0$) the random variable (10), with $t_1^\Delta = \Delta$, is negative. The Monte Carlo estimate of the conditional probability is computed for various choices of η and $|x_\Delta - x_0|$ using 10^8 experiments each. (12) suggests that choosing $\eta = c\Delta^{\frac{3}{2}}l$ with $|x_\Delta - x_0| = d\Delta^{\frac{1}{2}}$ (for some positive constants c and d) results in constant bound. This is reflected by the straight line behaviour of the Data 1 in Figure 1. For contrast, the bound on the conditional probabilities are also illustrated. We also compute the bound when averaging over X_Δ . Combining the bound (12) with the expansion $\mathbb{I}_{[E_1 < 0]} \leq \mathbb{I}_{[E_1 < 0]} \mathbb{I}_{[\eta > \Delta l | X_\Delta - x_0]} + \mathbb{I}_{[\eta \leq \Delta l | X_\Delta - x_0]}$, we can compute the unqualified bound for $\Pr(E_1 < 0 | \kappa > 0)$ to be

$$(13) \quad \Pr(E_1 < 0 | \kappa > 0) \leq 2 + 4\Phi\left(\frac{2\eta}{\Delta^{\frac{3}{2}}l}\right) - 6\Phi\left(\frac{\eta}{\Delta^{\frac{3}{2}}l}\right)$$

where Φ is the CDF of a standard normal distribution. (The proof is provided in Appendix C.) In Section 4.1.1, we advocate a design choice of $\eta = \Delta l$ (with the Lipschitz constant estimated in a causal manner with the population of particles) to ensure the simulation cost decreases proportionally with the time discretisation Δ . An estimate of $\mathbb{E}\left\{\exp\left(-\int_0^T \lambda(X_t)dt\right)\right\}$ or

$$\mathbb{E}\left\{\exp\left(-\int_0^\Delta \lambda(X_t)dt\right) \cdots \exp\left(-\int_{\lfloor \frac{T}{\Delta} \rfloor \Delta}^T \lambda(X_t)dt\right)\right\}$$

will entail the product of T/Δ (conditionally independent) estimates for the individual intervals. Using (13), this estimate is negative with a probability no greater than $\Pr(E_1 < 0 | \kappa > 0) \times T/\Delta$. Figure 2 illustrates how the bound in (13), when multiplied with T/Δ , decays with the choice $\eta = \Delta l$.

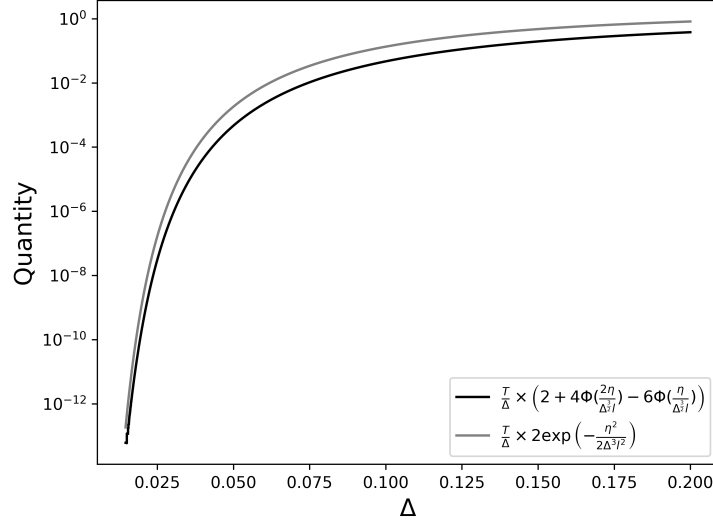


FIGURE 2. Plot of (13) multiplied by T/Δ vs. Δ for the design choice of $\eta = \Delta l$ when $T = 1$ with fitted relationship.

4.1.1. *Design choice for (η, Δ) .* We employ a reasoning similar to the above to bound the probability Algorithm 3 encounters a negative Poisson estimate. For a step-size Δ , an N -particle implementation has $\lceil T/\Delta \rceil$ forward steps and the event of encountering at least one negative Poisson estimate is $\left\{ \bigcup_{n=1}^N \bigcup_{i=1}^{\lceil T/\Delta \rceil} \{E_i^{(n)} < 0\} \right\}$. Using Lemma 1, its probability may be bounded above by the union bound,

$$\Pr \left(\bigcup_{n=1}^N \bigcup_{i=1}^{\lceil T/\Delta \rceil} \{E_i^{(n)} < 0\} \right) \leq \sum_{n=1}^N \sum_{i=1}^{\lceil T/\Delta \rceil} \Pr \left(E_i^{(n)} < 0 \right) < N \left\lceil \frac{T}{\Delta} \right\rceil \times 2 \exp \left\{ -\frac{\frac{2\eta}{\Delta l} \left(\frac{\eta}{\Delta l} - d\sqrt{\Delta} \right)}{\Delta} \right\}$$

where we have assumed that $|x_\Delta - x_{(i-1)\Delta}| \leq d\sqrt{\Delta}$, for all $i \in \{1 : \lceil T/\Delta \rceil\}$, for some constant $d > 0$ and $\eta/(\Delta l) > d\sqrt{\Delta}$. (A similar heuristic could also be found using (13).) We can make a design choice for η and Δ (within the constraints $\eta \geq \Delta^{\frac{3}{2}}l$ and $\eta/(\Delta l) > d\sqrt{\Delta}$) to ensure the probability of encountering a negative estimate is at most ϵ ,

$$(14) \quad \left\lceil \frac{NT}{\Delta} \right\rceil \times 2 \exp \left\{ -\frac{\frac{2\eta}{\Delta l} \left(\frac{\eta}{\Delta l} - d\sqrt{\Delta} \right)}{\Delta} \right\} \leq \epsilon.$$

For example, using $\eta = \Delta l$, the bound will fall below ϵ once Δ is small enough, say $\Delta = \bar{\Delta}$, and will continue to hold as Δ is decreased further since the left hand side decreases as Δ decreases. A similar heuristic could also be found using (13). In summary, set $\eta = \Delta l$ and

$$(15) \quad \Delta = \sup \{ \Delta > 0 : (14) \text{ and } \lceil NT/\Delta \rceil \times (13) \leq \epsilon \}$$

One can apply numerical methods such as Newton's method to solve (14). Also, ϵ can be exceptionally small, for example, $\Delta = 0.01$, $NT = 10^4$, $d = 3$ and $\eta = \Delta l$ yields $\epsilon \approx 10^{-55}$.

The design choice $\eta_k = \Delta \hat{l}_{k-1}$ can be computed sequentially in Algorithm 3. \hat{l}_{k-1} is the empirical Lipschitz constant updated sequentially as follows

$$(16) \quad \hat{l}_k := \max \left\{ \max_{i \in \{1:N\}} \frac{|\lambda(X_{t_k^\Delta}^{(i)}) - \lambda(X_{t_{k-1}^\Delta}^{(i)})|}{|X_{t_k^\Delta}^{(i)} - X_{t_{k-1}^\Delta}^{(i)}|}, \hat{l}_{k-1} \right\}$$

where the initial estimate \hat{l}_0 can be chosen to be the maximum ratio estimate as in (16) but computed with the particle set at time t_0^Δ only and the maximum is found over $i \neq j \in \{1 : N\}$. These design choices for \hat{l}_k and η_k for Algorithm 3 are used in all the numerical experiments presented in Section 5.

4.1.2. *Truncation Bias.* In Algorithm 3, we truncate the negative Poisson estimates to zero which will induce a bias. Hence we wish to study the bias of this truncated estimate for time discretisation, $0 < \Delta < \dots < m\Delta = T$ when Δ approaches zero, i.e.

$$\mathbb{E} \left\{ \exp \left(- \int_0^T \lambda(X_s) ds \right) \right\} - \mathbb{E} \{ E_1^+ \dots E_m^+ \}.$$

where $E_i^+ = E_i \mathbb{I}_{A_i^c}$ is the truncated Poisson estimate and A_i denotes the event $E_i < 0$. To do so, we can bound the omitted term $\mathbb{I}_A \prod_{i=1}^m E_i$ where $A = A_1 \cup \dots \cup A_m$ using the following lemma.

Lemma 2. *Let $\{X_s\}_{0 \leq s \leq \Delta}$ be one dimensional Brownian motion which starts at $X_0 = x_0$. Let $\lambda(\cdot)$ be a non-negative l -Lipschitz function and consider the estimate of the path integral*

$$\mathbb{E} \left\{ \exp \left(- \int_0^\Delta \lambda(X_t) dt \right) \dots \exp \left(- \int_{(m-1)\Delta}^{m\Delta} \lambda(X_t) dt \right) \right\} = \mathbb{E} \{ E_1 \dots E_m \},$$

where $(E_{i+1}, X_{(i+1)\Delta}) \leftarrow \text{PE}(\Delta l, i\Delta, (i+1)\Delta, X_{i\Delta})$ (see Algorithm 2) for $i = 0, \dots, m-1$. Then the following bound holds,

$$\left| \mathbb{E} \left\{ \mathbb{I}_A \prod_{i=1}^m E_i \right\} \right| \leq \exp\left(\frac{Tl}{2}\right) \times \left(\frac{1+4\Delta^2 l}{1-4\Delta^2 l}\right)^{\frac{m}{2}} \times m^{\frac{1}{2}} \left[2 \exp\left(-\frac{1}{2\Delta}\right) \right]^{\frac{1}{2}}.$$

Proof. See Appendix D. □

For $m = T/\Delta$, the second (ratio) term in the product recedes quickly to one as Δ approaches 0, which implies the final term dominates the bias. For $m = T/\Delta$, the final term also tends to 0. Based on this result, as an indicative trend, the square of the relative bias (which contributes additively in the relative MSE calculation) of Algorithm 3 is of the order

$$\frac{(\mathcal{L} - \mathbb{E}(\hat{\mathcal{L}}))^2}{\mathcal{L}^2} \leq \text{const}(T) \times \frac{1}{\Delta} \exp\left(-\frac{1}{2\Delta}\right).$$

where $\hat{\mathcal{L}}$ is (11). This result is commented on further in Section 5.1.

4.1.3. *Further comments.* The following idea, based on *Wald's identity* for sampling, was employed in [13] to deal with negative weights in particle filtering. We describe it here in the context of a single step within particle filtering and discuss its implications for estimating the likelihood. Consider $X_0 \sim \nu^\theta$ and let $G^\theta(x_0)$ be a non-negative function, also assumed θ dependent, and the aim is to estimate the likelihood $L(\theta) = \mathbb{E}^\theta(G^\theta(X_0))$. Assume there exists an unbiased estimate of $G^\theta(x_0)$ for any (θ, x_0) defined as follows. Let $p^\theta(e|x_0)$ be a conditional pdf on the real line with mean $\int_{-\infty}^{\infty} ep^\theta(e|x_0)de = G^\theta(x_0)$. Given X_0 , let $E^{(i)}$, $i = 1, 2, \dots$, be independent samples from $p^\theta(e|X_0)$ and let $K = \inf \{k > 0 : E^{(1)} + \dots + E^{(k)} > 0\}$. Then $\hat{L} = \sum_{i=1}^K E^{(i)}$ has mean

$$\mathbb{E}^\theta(\hat{L}) = \mathbb{E}^\theta(G^\theta(X_0)\mathbb{E}^\theta(K|X_0)) \neq L(\theta) \times \text{constant}$$

where product $G^\theta(X_0)\mathbb{E}^\theta(K|X_0)$ is Wald's identity, $\mathbb{E}^\theta(K|X_0)$ is the mean of the number of independent draws needed to ensure positivity and the constant on the right is θ independent; a θ independent constant is needed for the method to be used for model calibration.

This approach of sampling until the estimate is positive was proposed in [13] to address the event that a negative estimate is returned by $p^\theta(e|X_0)$. The constant $\mathbb{E}^\theta(K|X_0)$ seems to play no role in a particle filtering algorithm, since the weights are normalised before used as an input to the resampling step. However $\mathbb{E}^\theta(K|X_0)$, which is clearly X_0 dependent, can be θ dependent as well, e.g. as it would for $G^\theta(x_0) = \mathbb{E}_{x_0}^\theta \{ \exp(-\int_0^\Delta \lambda(X_s)ds) \}$ and its estimate $E^{(i)}$ returned by Algorithm 2 (for $\text{PE}(\eta, 0, \Delta, x_0)$) since K would depend on the law of $\{X_t\}_t$. Also, the function $G^\theta(x_0)$ can be θ dependent. As there is no easy way to compute or remove this factor $\mathbb{E}^\theta(K|X_0)$, this precludes its use within e.g. a PMMH sampler which require a (positive) unbiased estimator of $L(\theta)$ to generate MCMC samples from the posterior density of the model parameters θ . We provide some experiments in Appendix E to show that the idea of Wald's identity for sampling returns biased estimates.

We note finally that it is possible to adapt our approach slightly to return (perfectly) unbiased estimates. Recall that a particle filter such as Algorithm 3 may return an unbiased estimate of not only the normalising constant, but more generally of any unnormalised path expectation [9]; that is, the quantity

$$(17) \quad \hat{\mathcal{L}} \times \frac{\sum_{i=1}^N W_m^{(i)} \varphi(X_{t_0^\Delta}^{(i)}, \dots, X_{t_m^\Delta}^{(i)})}{\sum_{i=1}^N W_m^{(i)}}$$

is an unbiased estimate of

$$\mathbb{E} \left\{ \left(\prod_{i=1}^{n_p} \lambda(X_{t_i}) g^\theta(y_{t_i}|X_{t_i}) \right) \Psi(X_{t_0^\Delta}, \dots, X_{t_m^\Delta}) \times \varphi(X_{t_0^\Delta}, \dots, X_{t_m^\Delta}) \right\}$$

where $\Psi(\cdot)$ is the expectation of a product of Poisson estimates of the form $\prod_{i=1}^m \max(0, E_i)$. This quantity would be equal to $\exp\left(-\int_0^T \lambda(X_s)ds\right)$ if we could replace each truncated estimate $\max(0, E_i)$ by the estimate E_i itself.

We may use this to estimate unbiasedly the marginal likelihood of an alternative model, based on a different likelihood for the data (given the states). In particular, consider a variant of Algorithm 3 where $\max\{E_k^{(i)}, 0\}$ is replaced by $|E_k^{(i)}|$ in line 11. (Adapt the definition of Ψ accordingly.) The weights remain non-negative, and the output remains biased (for estimating the true likelihood \mathcal{L}). In (17), replace $\varphi(\cdot)$ by $(-1)^n$, where n is the number of negative Poisson estimates E_k that have occurred while constructing the considered trajectory (the argument of $\varphi(\cdot)$). It is easy to see that this is an unbiased estimate of the true likelihood \mathcal{L} . (Formally, φ is then a function of both the state trajectory and the E_k variables that have been generated while constructing that trajectory in this case).

In our numerical experiments, it was easy to set up the tuning parameters to make the number of occurrences of negative weights equal to virtually zero, so we could not observe any practical benefit in removing (entirely) the bias. However, this approach may be kept in mind for more complicated scenarios.

5. NUMERICAL EXPERIMENTS

In this section, we present numerical examples to compare Algorithm 1 and Algorithm 3 for likelihood estimation, smoothing and model calibration using Particle MCMC.

5.1. 1D example with exact calculation. We first consider a simple example in which the state X_t is a one dimensional Brownian motion and X_t is observed in zero mean unit variance Gaussian noise. The intensity function of the Cox process is $\lambda(x) = x + 10$. The state starts at $x_0 = 0$ at time $t = 0$ and the record of observations stops at time $T = 2$.

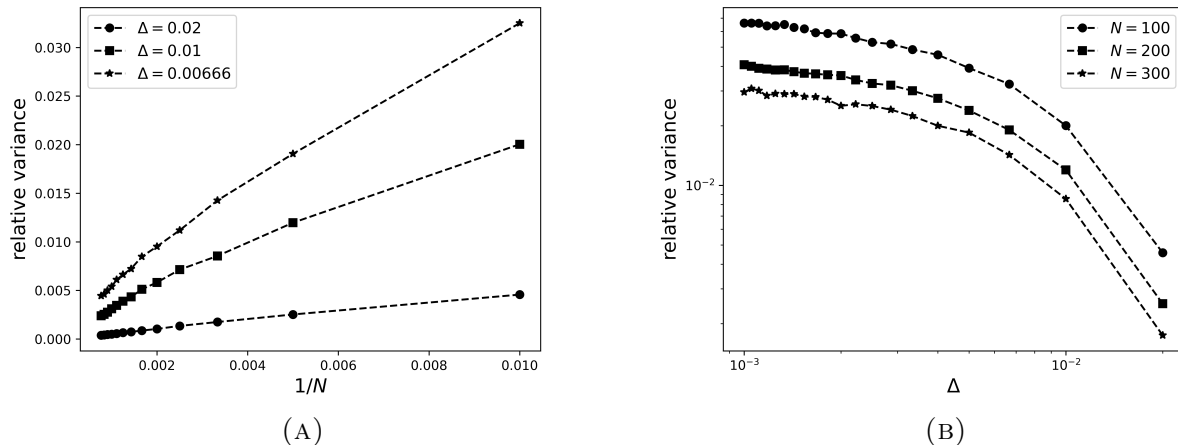


FIGURE 3. Plot of relative variance, defined to be $\mathbb{E}\{(\hat{\mathcal{L}}_\Delta)^2\}/\mathcal{L}_\Delta^2 - 1$, for $\hat{\mathcal{L}}_\Delta$ given by Algorithm 1. In (a) versus $1/N$ and in (b) as Δ varies on a log scale.

The integration that defines this likelihood can be computed exactly and thus can serve as ground truth; see Appendix F. We assume we observe $n_p = 2$ data-points, to make it possible to do a large number of runs; see Appendix H for extra results with $n_p > 2$.

For the analysis below, we use the relative mean squared error (rMSE) as the metric to measure the quality of likelihood estimates. Numerical results displayed in Figure 3a shows that the estimate of \mathcal{L}_Δ given by Algorithm 1, for any Δ , has a relative variance which is inversely proportional to the number of particles N used in the particle filter, where the relative variance defined to be $\mathbb{E}\{(\hat{\mathcal{L}}_\Delta)^2\}/\mathcal{L}_\Delta^2 - 1$. (We note though that the slope varies very slightly with $1/N$.) In Figure 3b, as expected, the relative variance for a fixed N stabilises as Δ decreases. (This reason is that a time-discretised particle system with systematic resampling converges to a continuous time limit as Δ approaches zero, as recently shown in [7].) For any sufficiently smooth function $\lambda(\cdot)$, the weak error of Euler scheme (i.e. relative bias $(\mathcal{L}_\Delta/\mathcal{L}) - 1$ in our case) is at most of order Δ [20, Chapter 17]. Overall, this implies the following empirical relationship for all values of n_p when Δ is small:

$$(18) \quad \text{rMSE} = \frac{1}{\mathcal{L}^2} \mathbb{E} \left\{ \left(\hat{\mathcal{L}}_\Delta - \mathcal{L} \right)^2 \right\} = \frac{c_1}{N} + c_2 \Delta^2 = \frac{c_1}{\mathcal{C}\Delta} + c_2 \Delta^2$$

where \mathcal{C} denotes the CPU time spent to run the particle filter (Algorithm 1) to completion. In the last equality, we use the relationship that \mathcal{C} increases linearly with NT/Δ which corresponds to T/Δ propagation steps for N particles. (Figure 4 confirms (18).) For fixed CPU time of \mathcal{C} , the value of Δ that minimises the relative MSE is $\Delta^* = \left(\frac{c_1}{c_2 \mathcal{C}} \right)^{\frac{1}{3}}$. Substituting this Δ^* into (18) gives the best relative MSE value for each \mathcal{C} , which is of order $\mathcal{O}(\mathcal{C}^{-\frac{2}{3}})$ and confirmed in Figure 5. Similarly, we can apply the same idea to determine Δ that minimises the relative MSE for Algorithm 3,

$$(19) \quad \text{rMSE} \leq \frac{c_1}{N} + \frac{c_2}{\Delta} \exp\left(-\frac{1}{2\Delta}\right) = \frac{c_1}{\mathcal{C}\Delta} + \frac{c_2}{\Delta} \exp\left(-\frac{1}{2\Delta}\right)$$

Since the minimisation problem above cannot be solved exactly, one can pursue a surrogate for Δ^* , in its vicinity, by minimising

$$f(\Delta) = \frac{c_1}{\mathcal{C}\Delta} + c_2 \exp\left(-\frac{1}{2\Delta}\right).$$

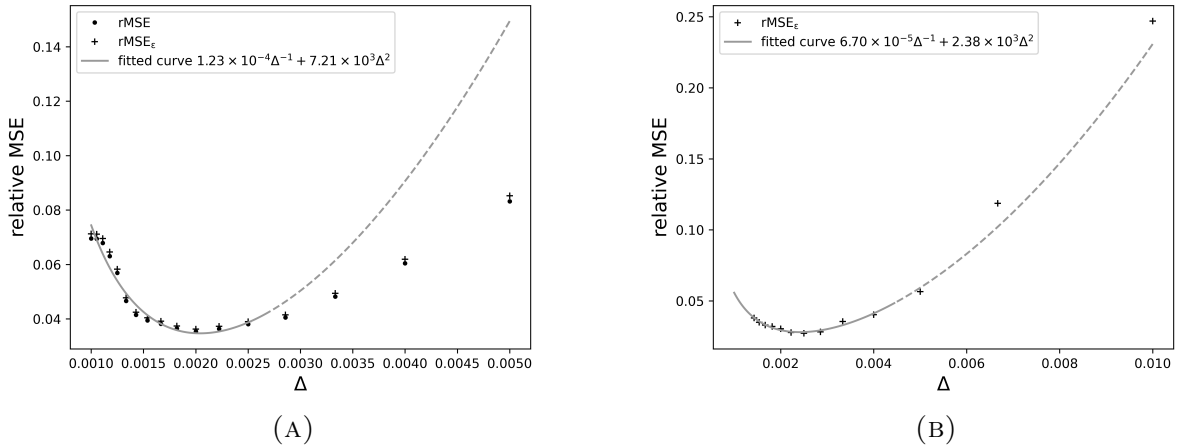


FIGURE 4. Plot of relative MSE versus Δ for fixed 1.5s CPU time for likelihood estimates computed by Algorithm 1 (using (6)) for (a) $n_p = 2$ and (b) $n_p = 13$. Overlaid is the fitted relationship in (18) to a range of Δ values around the minimum of rMSE, illustrated by the solid segment of the line. The dashed segment cover data points there were not used in fitting. The coefficients of the fitted curve to rMSE $_\epsilon$ are only 2.4% different to that of the rMSE data points, hence it would be indistinguishable graphically.

Note that $\text{rMSE}(\Delta) > f(\Delta)$, $\forall 0 < \Delta < 1$. Minimising this equation gives $\Delta^* = \left(2 \log \left(\frac{c_2 \mathcal{C}}{2c_1}\right)\right)^{-1}$. Hence Δ^* , not being the true minimiser of (19), is a more conservative solution. Substituting this Δ^* into (19) gives an indication of the best relative MSE value for each \mathcal{C} , which is of order of $\mathcal{O}(\mathcal{C}^{-1} \log(\mathcal{C}))$. In practice, we do not recommend this optimisation but rather choose (Δ, η) as detailed in Section 4.1.1 and then stick to this choice even if more CPU time \mathcal{C} has become available. We define rMSE $_\epsilon$ to be (18) with \mathcal{L} replaced with $\mathcal{L}_{\text{MC}} = \mathcal{L} + \epsilon$. Recall we denote by \mathcal{L}_{MC} the Monte Carlo estimate returned by the modified Algorithm 3 which uses the true path integral given by (30) in Appendix rather than Poisson estimate. We ensure the Monte Carlo error ϵ is small enough so that our conclusions in comparing the accuracy of Algorithms 1 and 3 are not rendered inaccurate for the case $n_p > 2$ studied below. We use the $n_p = 2$ case to choose a value of ϵ that ensures the best Δ found using rMSE $_\epsilon$ is close enough to the desired (best) Δ for rMSE.

Continuing with for $n_p = 2$, Figure 4a reports the rMSE and rMSE $_\epsilon$ of Algorithm 1 for a fix CPU budget and different Δ values with the expected relationship in (18) fitted to a range of Δ values around the minimum. rMSE $_\epsilon$ uses \mathcal{L}_{MC} which is the average estimate of \mathcal{L} given by 10^6 runs of modified Algorithm 3 with each run using $N = 10^6$ particles. We calculate the relative error between Δ_ϵ^* and Δ^* , and between rMSE $_\epsilon(\Delta_\epsilon^*)$ and rMSE(Δ^*), using their fitted c_1 's and c_2 's values,

$$\left| \frac{\Delta_\epsilon^* - \Delta^*}{\Delta^*} \right| = 1.1 \times 10^{-9}, \quad \left| \frac{\text{rMSE}_\epsilon(\Delta_\epsilon^*) - \text{rMSE}(\Delta^*)}{\text{rMSE}(\Delta^*)} \right| = 0.024.$$

This shows that 10^6 -averaged runs of modified Algorithm 3 with $N = 10^6$ particles is more than sufficient to produce accurate estimate \mathcal{L}_{MC} as the substitute of \mathcal{L} . We used the same number of Monte Carlo repetitions and N for values of $n_p > 2$ up to $n_p = 13$, which are reported in Figure 4b. Both Figure 4a and 4b validate the expression for the rMSE (18)

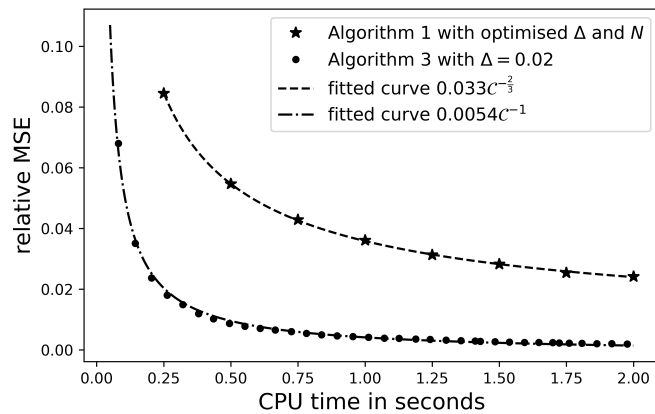


FIGURE 5. Comparison between likelihood estimates computed by Algorithm 1 (using (6)) and by Algorithm 3 (using (11)). The true likelihood is approximated with Algorithm 3 using $N = 10^4$ particles and $\Delta = 0.02$. Note that Algorithm 1 uses optimised Δ and N to obtain the best MSE for a given CPU budget. Algorithm 3 uses fixed Δ value $\Delta = 0.02$ and the design choice for η described in Section 4.1.1.

in the locality of the minimum Δ . We continue to use \mathcal{L}_{MC} to compare Algorithms 1 and 3. We use \mathcal{L}_{MC} to find the smallest relative MSE Algorithm 1 can achieve for a given CPU budget, while we use \mathcal{L}_{MC} to compute the relative MSE of Algorithm 3 for the same CPU budget. For Algorithm 1, for each value of \mathcal{C} , we repeat the procedure illustrated in Figure 4 to find the Δ that yields the smallest rMSE_e – this Δ is the minimiser of the fitted line as illustrated in Figure 4b. For Algorithm 3, we spend the budget on increasing the number of particles N while using a fixed Δ value of $\Delta = 0.02$. The results of this comparison are shown in Figure 5. It appears that Algorithm 3 achieves the best decay rate of rMSE with CPU budget, which is the inverse relationship, whereas Algorithm 1 can only achieve a rate of $\mathcal{C}^{-2/3}$.

5.2. 3D Single Molecule Model. In this section we apply our methodology to track a moving biological molecule (biomolecule) in a live cell, in three dimensions, arising from single molecule fluorescence microscopy. An illustration of how the data is generated is given Figure 6. Single molecule fluorescence microscopy is a live cell imaging technique where biomolecules of interest are tagged with a fluorophore, which are then excited with light at a particular frequency. These molecules fluoresce under excitation and emit light a different frequency, which is then captured by a CCD camera after optical magnification. The recorded images are used to uncover their motion. A mathematical abstraction of the problem is precisely the model in Section 2.2, see also [25] and [8]. In particular, the moving molecule follows a diffusion model and its observations are the (random) arrival times and locations of individual photons. The data are both the arrival times and locations of the photons. The photon arrival times are governed by the depth of the molecule (see Figure 8) as the excitation of the molecule varies inversely with the molecule’s depth due to the attenuation of the excitation light. Photon arrival locations are imprecise (noise corrupted) observations of the molecule’s location in the other two dimensions as governed by diffraction theory. The relevant photon location model is the Born and Wolf model for the point spread function, which describes how a point light source appears in an image as it moves in and out of focus [25]. We let $(X_t)_{0 \leq t \leq T} := (X_{1,t}, X_{2,t}, X_{3,t})_{0 \leq t \leq T}^\top$ denote

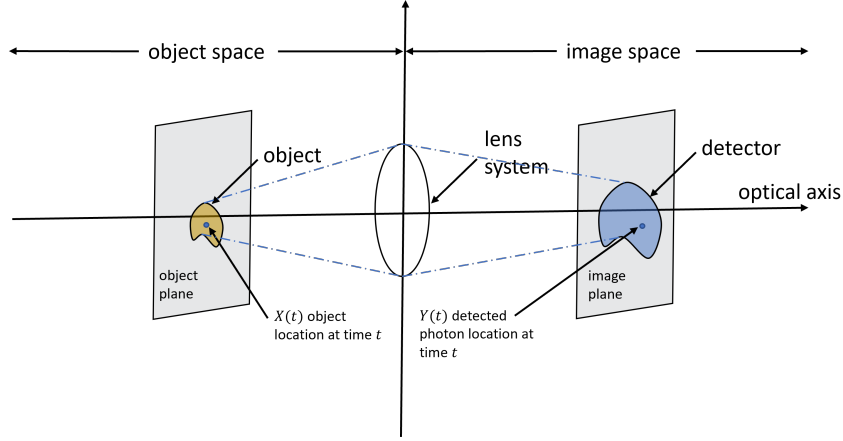


FIGURE 6. Illustration of the setup about how the image is acquired by a microscope. $X(t)$ denotes the object location at time t and $Y(t)$ denotes the detected photon location at time t .

the true, 3-dimensional location of the molecule at time t . The three components of the molecule state, i.e. $(X_{1,t}, X_{2,t}, X_{3,t})_{0 \leq t \leq T}^\top$, are its $(x, y, z)^\top$ location and assumed to follow the *Ornstein-Uhlenbeck* (O-U) model,

$$dX_{i,t} = -\phi_i(X_{i,t} - \mu_i)dt + dW_{i,t}, \quad \text{for } i = 1, 2, 3$$

where $\phi_i > 0$ and $(W_{i,t})_{0 \leq t \leq T}$, $i = 1, 2, 3$, are independent Brownian motions. We assume that the initial distribution which generates X_0 is $\mathcal{N}(\mu, \Sigma_0)$, where the covariance matrix $\Sigma_0 = p_0 \times \mathbb{I}_{3 \times 3}$. The transition density $f_\delta^\theta(x'|x)$ of the process can be expressed as follows,

$$(20) \quad X_{i,t+\delta} | (X_{i,t} = x_i) \sim \mathcal{N}\left(\mu_i + e^{-\delta\phi_i}(x_i - \mu_i), \frac{1}{2\phi_i}(1 - e^{-2\delta\phi_i})\right), \quad i = 1, 2, 3.$$

For an object located at $(x_1, x_2, x_3)^\top \in \mathbb{R}^3$ in the object space (prior to magnification), the location (on the detector) at which a photon is detected is specified probabilistically with $2D$ probability density function,

$$(21) \quad g^\theta(y|x) := \frac{1}{|M|} q_{x_3}(M^{-1}y - (x_1, x_2)^\top), \quad y \in \mathbb{R}^2$$

where $M \in \mathbb{R}^{2 \times 2}$ is an invertible lateral magnification matrix and the image function $q_{x_3} : \mathbb{R}^2 \rightarrow \mathbb{R}$ describes the image of an object in the detector space when that object is located at $(0, 0, x_3)$ in the object space, where $x_3 \in \mathbb{R}$ is the location of the object on the optical axis. This 3D Born and Wolf model is the resulting image function, derived from diffraction theory, for a point source that can also be out of focus [6]. For $(x_1, x_2) \in \mathbb{R}^2$,

$$(22) \quad q_{x_3}(x_1, x_2) = \frac{4\pi n_\alpha^2}{\lambda_e^2} \left| \int_0^1 J_0\left(\frac{2\pi n_\alpha}{\lambda_e} \sqrt{x_1^2 + x_2^2} \rho\right) \exp\left(\frac{j\pi n_\alpha^2 x_3}{n_0 \lambda_e} \rho^2\right) \rho d\rho \right|^2,$$

where n_0 is the refractive index of the objective lens immersion medium and n_α is the numerical aperture of the objective lens. λ_e is the emission wavelength of the molecule. $J_0(\cdot)$ and $J_1(\cdot)$ represents the zero-th order and the first order Bessel function of the first kind, respectively. The probability density functions of Born and Wolf model at different defocus levels are plotted in Figure 7. A large defocus tends to produce images of poor quality and this will further pose difficulty in estimating the molecule's position.

The time instances at which the photons arrive on the detector are random as well, and the photon emission process is modelled as a Poisson process [25]. The photon rate, denoted

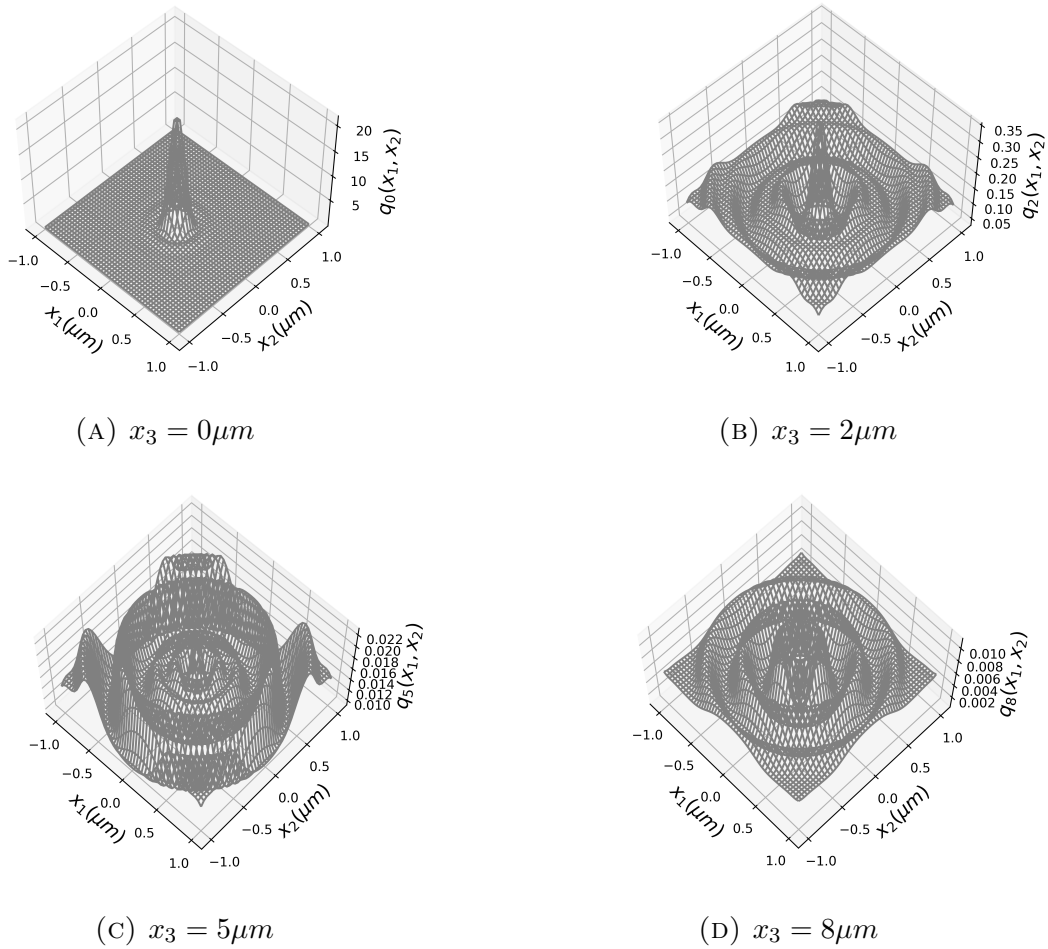


FIGURE 7. Born and Wolf point spread function at different defocus levels. Mesh representations are shown for (22) at different defocuses x_3 , computed with wavelength $\lambda_e = 0.52\mu m$, numerical aperture $n_\alpha = 1.4$, refractive index of the objective lens immersion medium $n_0 = 1.515$. The x_3 values shown correspond to point source positions (a) $x_3 = 0\mu m$ (in focus), (b) $2\mu m$, (c) $5\mu m$ and (d) $8\mu m$.

as $\lambda(t)$, is the rate at which photons are emitted by the object at time t is often assumed to be constant. For example, [8] and [31] applied particle filtering to jointly calibrate the model and localise the single molecule under the assumption that the molecule is static on the optical axis, or at least their movement on the optical axis has an insignificant effect on the photon rate. In contrast to their modelling assumption, we follow the approach of [30] to incorporate movement in all three coordinates. The molecule's depth affects the photon arrival rate and arrival locations, the former through a state (depth) dependent photon detection rate $\lambda(X_t)$ and the latter through the 3D Born and Wolf model. Figure 8 illustrates the total internal reflection phenomenon. For comprehensive review, see [2]. This phenomenon is caused by the surface-associated evanescent electromagnetic field that is generated when an excitation beam is internally reflected at a planar interface between two transparent media with different refractive indices, n_1 and n_2 . [30] have shown that the photon detection rate $\lambda(\cdot)$ decays exponentially along x_3 -axis, $\lambda(x_3) = \lambda_0 \exp(-\frac{x_3}{d})$, where λ_0 denotes the rate of photons emitted by a fluorophore at $x_3 = 0$. Under this set-up,

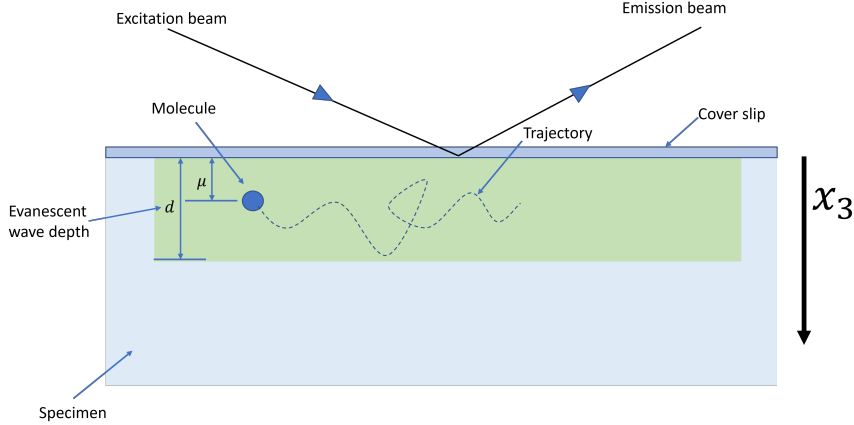


FIGURE 8. Total internal reflection fluorescence. An excitation beam with wavelength λ_v traveling from a high refractive index (n_1) medium into a lower refractive index (n_2) medium is totally internal reflected at a planar interface. The reflection generates a thin layer of light in the lower refractive index medium, whose intensity decays exponentially along the x_3 -axis with a characteristic constant d . While the molecule moves in the field, it is illuminated/excited and thus fluoresces. Parameter μ along x_3 -direction is the mean of $X_{3,t}$ which the molecule diffuses about.

one could consider x_3 -movement of a single molecule as a *reflected diffusion process* since the molecule should reflect when it encounters the cover slip. However, there is no practical approach available for exact simulation of this reflected process. For instance, [5]’s approach requires infinite expected running time, hence impractical when adapting into the particle filtering algorithms. We adopt a simpler approach by assuming standard O-U process which would be suitable if the molecule does not encounter a boundary (i.e. either cover slip $x_3 = 0$ or its maximum depth d) over its observation period, e.g. if the observation periods are short and/or the molecule is diffusing about a mean depth μ in the middle of the cell with large ϕ_3 (i.e. stronger attraction to μ), see Figure 8. In Figure 9a, we plot the true trajectory of the molecule for the numerical studies, which is generated by the SDE in (20) with parameters $\{\phi = (\phi_1, \phi_2, \phi_3)^\top = (1, 1, 4)^\top, \mu = (\mu_1, \mu_2, \mu_3)^\top = (0, 0, 2)^\top, p_0 = 1/(2\phi)\}$ for the time interval $[0, 5.0]$. The initial variance p_0 is set to be the stationary variance. We used a thinning algorithm (Algorithm 4 detailed in Appendix I) to generate the observation times by using the intensity function (see (5.2)) with parameters $\{\lambda_0 = 100, d = 20\mu\text{m}\}$. Given these observation times, we generate the observed photon locations with the photon distribution profile given by (21) and (22). The associated parameters are $\{M = m\mathbb{I}_{2 \times 2}, m = 100, n_\alpha = 1.4, \lambda_e = 0.52\mu\text{m}, n_0 = 1.515, \sigma_a^2 = 49 \times 10^{-4}\mu\text{m}^2\}$ and corresponding data set of photon locations is shown in Figure 9b. The colours in Figure 9a indicate time, and as described by the legend, the colours lighten with the progress of time. Figure 9c shows the mean of the estimated (X_1, X_2) locations of the molecule found using Algorithm 3, which does track the true trajectory. Figure 9d shows true X_3 position of the molecule, the mean of the estimated X_3 position (also obtained using Algorithm 3), along with the standard deviations. During periods when there are no observations, the estimated X_3 value is larger, as we would expect since this corresponds to a smaller photon arrival intensity function. Figure 9d also shows that large X_3 state values degrade the estimation quality (which is more clearly seen for the X_3 values). This is due to the Born and Wolf observation model

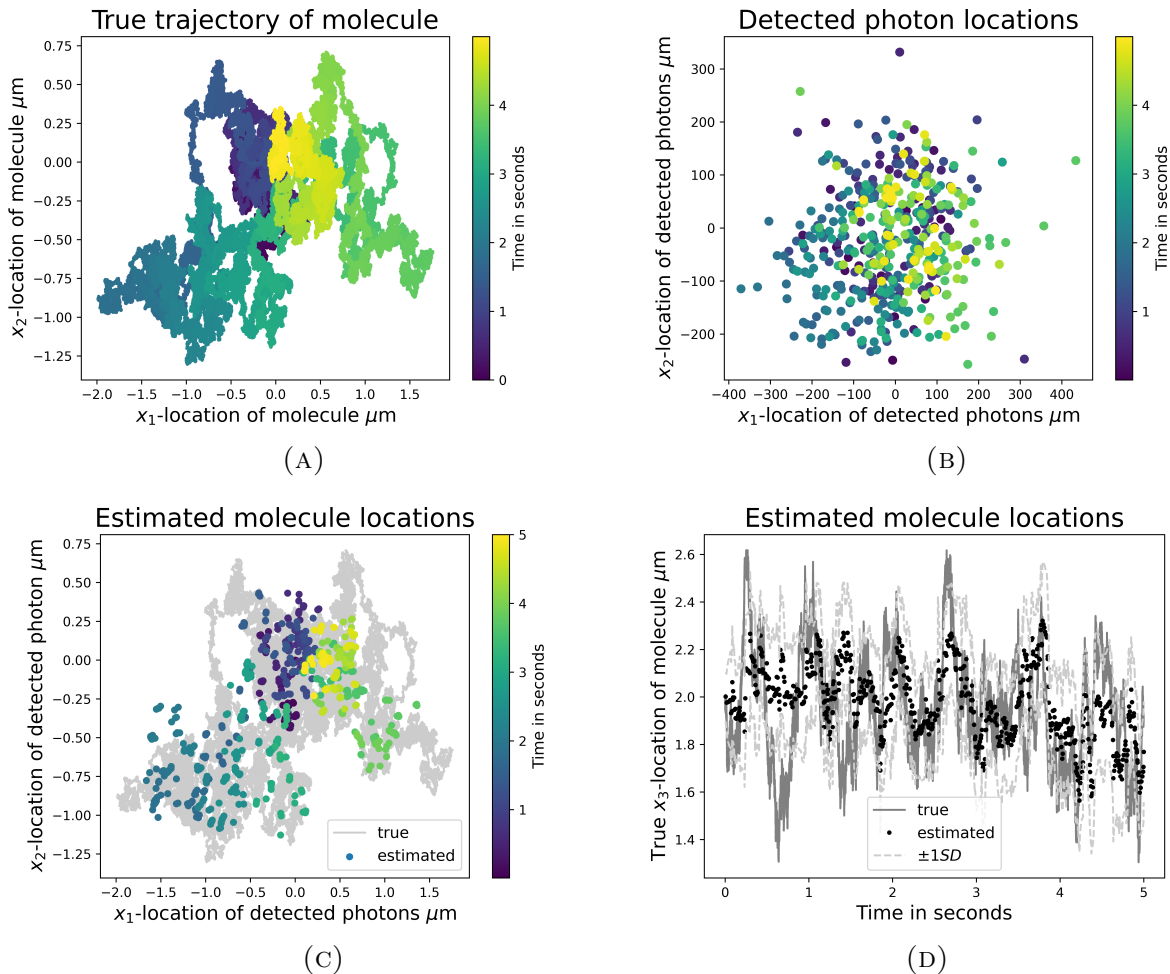


FIGURE 9. (a) True trajectory of a molecule; (b) observed photon locations; (c) estimated (x_1, x_2) molecule locations and (d) true x_3 molecule locations and estimated location.

for an out-of-focus molecule, see (22). Additional results of this phenomenon are reported in Appendix J.

Figure 10 shows a comparison between the estimation quality of Algorithms 1 (with $\Delta = 0.03, 0.003$ and 0.0003) and 3 (with $\Delta = 0.1$) for this single molecule example. For both methods, the CPU time is increased by increasing the number of particles used in the algorithms. The superiority of Algorithm 3 is apparent as measured using relative MSE of the likelihood estimate. As can be seen, the best Δ for Algorithm 1 is not necessarily the smallest one for a fix CPU budget. This also has practical consequences. For high frequency data, there will be potentially more time intervals between observation arrivals of which are much smaller than Δ . This would lead to a small bias for Algorithm 1 although at a higher computational cost. Further reducing the bias, the relative MSE would be dominated by the variance if the CPU budget only permits a smaller number of particles.

5.2.1. *Model calibration using PMCMC.* Estimating the parameters of the molecular dynamics is also important in single molecule studies. [8] calibrate the model using maximum likelihood estimation after discretising the path integral. In contrast, we use the particle marginal Metropolis-Hastings (PMMH) algorithm [1] to sample from the posterior density $p(\theta, x_{0:m}|y_{0:m})$ where $\theta = (\phi, \mu)$. Data is simulated from the model

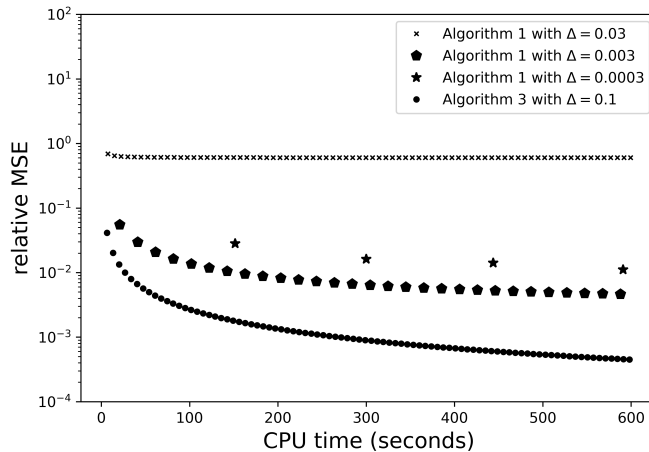


FIGURE 10. Plot of rMSE_ϵ of likelihood estimates versus CPU time for Algorithm 3 with $\Delta = 0.1$ and Algorithm 1 with $\Delta = 0.03, 0.003$ and 0.0003 . rMSE of likelihood estimates based on the average estimate of \mathcal{L} given by 10^6 runs of Algorithm 3 with each run using $N = 10^6$ particles, and the design choice for l and η given in Section 4.1.1. Here 600 CPU seconds corresponds to 2×10^5 particles for Algorithm 3.

$\{\phi = (1, 1, 4)^\top, \mu = (0, 0, 2)^\top, p_0 = (0.5, 0.5, 0.125)^\top\}^\top$ with intensity function parametrised by $\{\lambda_0 = 25, d = 20\}$. The parameters of the Born and Wolf model remain the same as before. Precise estimation of ϕ_3 requires a longer time series as it is weakly identified and we use 350 observations collected in the time interval $[0, 15s]$. The following independent priors are used: $\phi_3 \sim \mathcal{U}(0, 10)$ and $\mu_3 \sim \mathcal{U}(0, 10)$. (\mathcal{U} denotes the continuous uniform distribution.) We used a normal random-walk Metropolis Hastings proposal with initial covariance $0.1 \times \mathbb{I}_{2 \times 2}$ to update the parameters jointly. The continuous covariance adaptation scheme of [17] is adopted in the PMMH algorithm. We chose the following three experimental settings:

- Experiment 1 (low CPU budget): $\mathcal{C} = 1.5s$, which only allows a coarse time discretisation, which coincides with the time of arrivals of data for both Algorithms 1 and 3. This forces large Δ in \mathcal{L}_Δ for Algorithm 1. N is adjusted accordingly so that CPU budget is the same for both algorithms.
- Experiment 2 (larger CPU budget): $\mathcal{C} = 2.5s$ permits a finer time discretisation than the observation arrival times. The best Δ and N (within the CPU budget) are chosen for Algorithm 1 using the procedure outlined in Section 5.1. (Employing a larger CPU budget allows a smaller Δ than Experiment 1 in \mathcal{L}_Δ .) For Algorithm 3, we used $\Delta = 0.01$ and its CPU cost adjusted N .
- Experiment 3 (effective sample size based comparison): $\mathcal{C} = 2.0s$, the effective sample size (ESS) for PMMH using Algorithm 3 with $\Delta = 0.01$ is found, and then the best Δ and N are chosen for Algorithm 1 while ensuring its ESS matches that of Algorithm 3. The ESS, which measures the number of ‘independent samples,’ is

$$\text{ESS} = \frac{M}{-1 + 2 \sum_{t=0}^K (\rho_{2t} + \rho_{2t+1})}$$

where ρ_t is estimated autocorrelation at lag n and K is the last integer for which the sum in the sum bracket is still positive. The general trend is that the ESS of

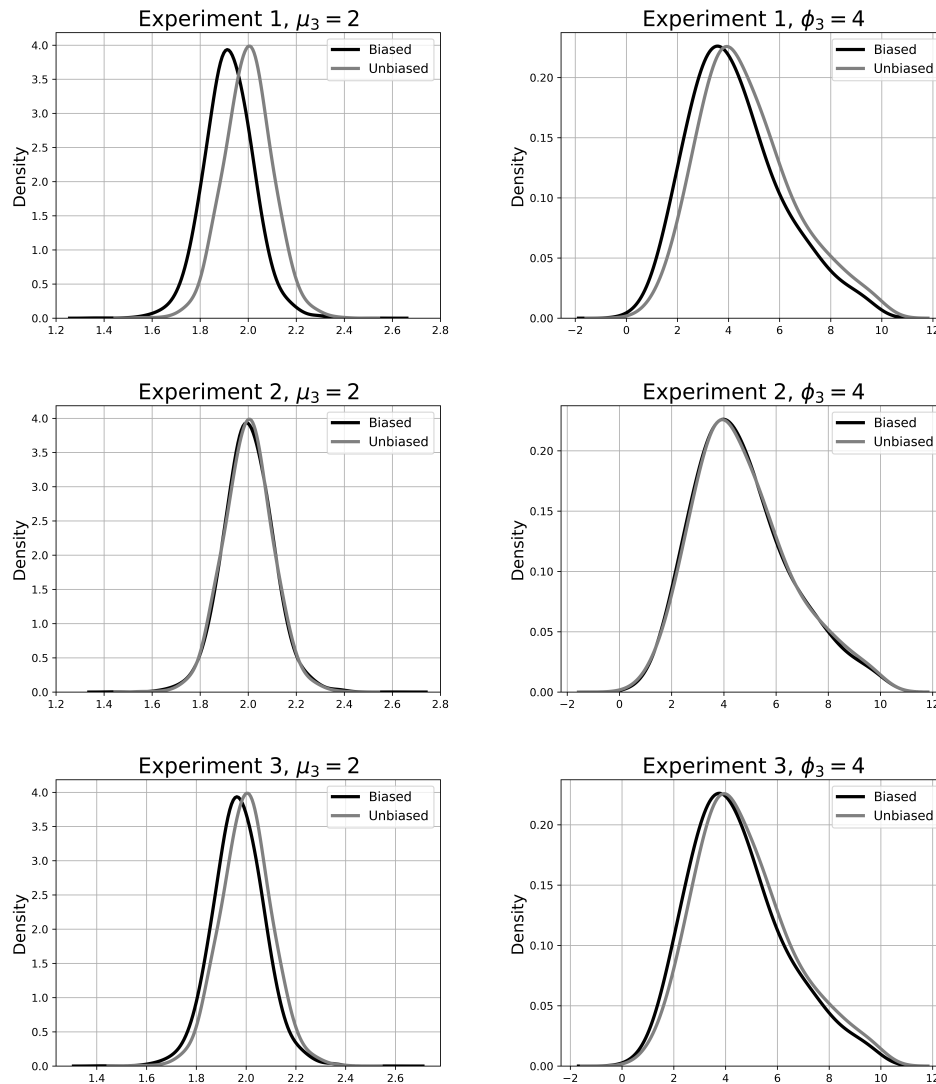


FIGURE 11. PMMH experiments: posterior densities $p(\mu_3|y_{t_1:t_{n_p}})$ and $p(\phi_3|y_{t_1:t_{n_p}})$ for experiment 1 in top panel, experiment 2 in middle panel and experiment 3 in bottom panel.

PMMH with Algorithm 1 increases when Δ is increased (i.e. larger N for the fixed CPU budget), although the estimation will be more biased for Algorithm 1.

We ran the algorithms for 10^5 with a 10^4 burn-in iterations. Figure 11 displays the estimates of the marginal posterior densities for μ_3 and ϕ_3 for all three experiments. Experiment 1 shows that Algorithm 3 effectively removes bias in the estimation of parameters while the performance of Algorithm 1 is compromised by the limited CPU budget. Experiment 2 shows that given sufficient budget Algorithm 1 is able to achieve almost the same performance of Algorithm 3. Comparison between experiments 1 and 2 show that the unbiased posterior produced by Algorithm 3 remain unaffected by the amount of available CPU budget. Experiment 3 is carried out under the setting that both algorithms produce equally “efficient” MCMC samples for a fix CPU budget, the result shows that Algorithm 1 still yields some amount of bias to the estimation.

6. CONCLUSION

In this paper we addressed the problem of smoothing and model calibration for a partially observed diffusion with a Cox process observation model. The intractable likelihood was estimated using the positive part of a Poisson estimate, for the path integrals within, embedded within particle filtering. The probability of encountering a negative Poisson estimate in one complete particle filtering pass through the data was strongly controlled by adjusting $\eta = \mathcal{O}(\Delta l)$. As such, due to the rarity of the occurrence of a negative estimate – which triggers the particle weight truncation – the time discretisation error which biases conventional particle implementations such as in [8] is effectively removed in this work. The numerical results showed that our proposed particle method (Algorithm 3) outperforms the conventional (discretisation-based) particle filter in terms of relative MSE, ours decaying with order $\mathcal{O}(\mathcal{C}^{-1})$ compared to $\mathcal{O}(\mathcal{C}^{-\frac{2}{3}})$ where \mathcal{C} is the computational budget. Our particle filter was then applied to a challenging three-dimensional single molecule microscopy example to estimate both the trajectory of the moving molecule and to calibrate the model. The bias in the posterior distribution for the model parameters computed using a conventional implementation like [8] was clearly illustrated, whereas in ours it was not discernible. Although the bias in the conventional method can be reduced by employing a smaller Δ , the time discretisation interval, this not only requires significant additional CPU time, it will also prohibit the application of backward sampling steps in particle filtering. This is a direction in which this work could be taken further, which is to define a forward filtering backward sampling implementation of our method. In the context of diffusions, this is a challenging problem, see [34] for a recent study.

APPENDIX A. BRIDGE DENSITY FOR LINEAR GAUSSIAN DIFFUSION

Consider the following stochastic differential equation (SDE),

$$(23) \quad dX_t = b(t, X_t)dt + \sigma(t, X_t)dW_t$$

where X_t is an n -dimensional diffusion process, W_t is an m -dimensional standard Brownian motion for $m \leq n$. For $b(t, X_t) := b_0 + b_1(t)X_t$ and $\sigma(t, X_t) := \sigma(t) \in \mathbb{R}^{n \times m}$, the solution to (23) at discrete time points $t_0 < t_1 < \dots$ is given by [11, 19]

$$(24) \quad X_{t_{i+1}} = \Phi(t_i, t_{i+1})X_{t_i} + a(t_i, t_{i+1}) + \int_{t_i}^{t_{i+1}} \Phi(t_i, t)\sigma(t)dW_t$$

where the fundamental matrix function $\Phi \in \mathbb{R}^{n \times n}$ satisfies the following for all $s, t, u \geq t_0$

$$\frac{d\Phi(s, t)}{dt} = b_1(t)\Phi(s, t), \quad \Phi(t, t) = \mathbb{I}_{n \times n}, \quad \Phi(s, t)\Phi(t, u) = \Phi(s, u),$$

the vector $a(t_i, t_{i+1}) \in \mathbb{R}^n$ is given by $a(t_i, t_{i+1}) = \int_{t_i}^{t_{i+1}} b_0\Phi(t_i, t)dt$. Therefore the transition density $f_{t_i, t_{i+1}}(x'|x)$ can be expressed as a Gaussian as follows,

$$\begin{aligned} f_{t_i, t_{i+1}}(x'|x) &:= \frac{\exp\left(-\frac{1}{2}(x' - \mu(x, t_i, t_{i+1}))^\top R^{-1}(t_i, t_{i+1})(x' - \mu(x, t_i, t_{i+1}))\right)}{\sqrt{|2\pi R^{-1}(t_i, t_{i+1})|}}, \\ &\propto \frac{\exp\left(-\frac{1}{2}(x - \hat{\mu}(x', t_i, t_{i+1}))^\top \hat{R}^{-1}(t_i, t_{i+1})(x - \hat{\mu}(x', t_i, t_{i+1}))\right)}{\sqrt{|2\pi \hat{R}^{-1}(t_i, t_{i+1})|}} \\ &:= \hat{f}_{t_i, t_{i+1}}(x|x'), \end{aligned}$$

where

$$\begin{aligned}\mu(x, t_i, t_{i+1}) &:= \Phi(t_i, t_{i+1})x + a(t_i, t_{i+1}), \\ \hat{\mu}(x', t_i, t_{i+1}) &:= \Phi^{-1}(t_i, t_{i+1})x' - \Phi^{-1}(t_i, t_{i+1})a, \\ R(t_i, t_{i+1}) &:= \int_{t_i}^{t_{i+1}} \Phi(t_i, t)\sigma(t)\sigma^\top(t)\Phi^\top(t_i, t)dt, \\ \hat{R}(t_i, t_{i+1}) &:= \int_{t_i}^{t_{i+1}} \Phi^{-1}(t, t_{i+1})\sigma(t)\sigma^\top(t)\Phi^{-\top}(t, t_{i+1})dt.\end{aligned}$$

Assume $s < \tau < t$, then in addition to sampling $p(x_\tau|x_s)$ exactly, one can also sample $X_\tau \sim p(x_\tau|x_s, x_t)$ exactly where

$$\begin{aligned}p(x_\tau|x_s, x_t) &\propto f_{s,\tau}(x_\tau|x_s)f_{\tau,t}(x_t|x_\tau) \propto f_{s,\tau}(x_\tau|x_s)\hat{f}_{\tau,t}(x_\tau|x_t) \\ &\propto \text{N}\left(x_\tau; \left(R^{-1}(s, \tau) + \hat{R}^{-1}(\tau, t)\right)^{-1} \left(R^{-1}(s, \tau)\mu(x_s, s, \tau) + \hat{R}^{-1}(\tau, t)\hat{\mu}(x_t, \tau, t)\right), \right. \\ &\quad \left. \left(R^{-1}(s, \tau) + \hat{R}^{-1}(\tau, t)\right)^{-1}\right).\end{aligned}$$

APPENDIX B. PROOF OF LEMMA 1

The following propositions will be used in the final proof.

Proposition 3. *Let X be the Brownian motion which starts at $X_0 = x_0$, then the following equality holds for any $a > 0$:*

$$\begin{aligned}\Pr\left(\sup_{0 \leq s \leq \Delta} X_s - X_0 \geq a | X_\Delta = x_\Delta\right) \\ = \begin{cases} \exp\left\{-\frac{2a}{\Delta}[a - (x_\Delta - x_0)]\right\}, & a > x_\Delta - x_0 \\ 1, & a \leq x_\Delta - x_0 \end{cases}\end{aligned}$$

Proof. Define τ_a as the hitting time of a as follows,

$$\tau_a = \inf\{s \in [0, \Delta] | X_s - X_0 = a\}$$

A hitting time is also a stopping time. Then by applying the reflection principle (please refer to Theorem 2.19 of [23]), the process $\{X^* : t \geq 0\}$, called Brownian motion $\{X_t : t \geq 0\}$ reflected at τ_a , defined by

$$\begin{aligned}X_t^* &= X_t \mathbb{I}_{t \leq \tau_a} + (2X_{\tau_a} - X_t) \mathbb{I}_{t > \tau_a} \\ &= X_t \mathbb{I}_{t \leq \tau_a} + (2a + 2x_0 - X_t) \mathbb{I}_{t > \tau_a}\end{aligned}$$

is also a Brownian motion. Thus,

$$\begin{aligned}&\Pr\left(\tau_a \leq \Delta, X_\Delta \in [x_\Delta, x_\Delta + dx]\right) \\ &= \Pr\left(X_\Delta^* \in [2a + 2x_0 - x_\Delta - dx, 2a + 2x_0 - x_\Delta]\right) \\ &= \Pr\left(X_\Delta^* - X_0 \in [2a + x_0 - x_\Delta - dx, 2a + x_0 - x_\Delta]\right) \\ &= \frac{dx}{\sqrt{2\pi\Delta}} \exp\left\{-\frac{[2a - (x_\Delta - x_0)]^2}{2\Delta}\right\}.\end{aligned}$$

Note that,

$$\begin{aligned} & \Pr\left(X_\Delta \in [x_\Delta, x_\Delta + dx]\right) \\ &= \Pr\left(X_\Delta - X_0 \in [x_\Delta - x_0, x_\Delta - x_0 + dx]\right) \\ &= \frac{dx}{\sqrt{2\pi\Delta}} \exp\left\{-\frac{(x_\Delta - x_0)^2}{2\Delta}\right\}. \end{aligned}$$

Division between two equations above concludes the proof. \square

Proposition 4. *Let X be the Brownian motion which starts at $X_0 = x_0$, then the following equality holds for any $a > 0$:*

$$\begin{aligned} & \Pr\left(\inf_{0 \leq s \leq \Delta} X_s - X_0 \leq -a \mid X_\Delta = x_\Delta\right) \\ &= \begin{cases} \exp\left\{-\frac{2a}{\Delta}[a + (x_\Delta - x_0)]\right\}, & a > -(x_\Delta - x_0) \\ 1, & a \leq -(x_\Delta - x_0). \end{cases} \end{aligned}$$

Proof. A similar approach as in Proof B but define $\tau_{-a} = \inf\{s \in [0, \Delta] \mid X_s - X_0 = -a\}$ and apply the reflection principle by defining the Brownian motion $\{X^* : t \geq 0\}$, the Brownian motion $\{X_t : t \geq 0\}$ reflected at τ_{-a} , formally defined by

$$X_t^* = X_t \mathbb{I}_{t \leq \tau_{-a}} + (-2a + 2x_0 - X_t) \mathbb{I}_{t > \tau_{-a}}.$$

\square

Proposition 5. *Let X be defined as in Proposition 3, then the following inequality holds:*

$$\begin{aligned} & \Pr\left(\sup_{0 \leq s \leq \Delta} |X_s - X_0| \geq a \mid X_\Delta = x_\Delta\right) \\ & \leq \begin{cases} 2 \exp\left\{-\frac{2a}{\Delta}[a - |x_\Delta - x_0|]\right\}, & a > |x_\Delta - x_0| \\ 1, & a < |x_\Delta - x_0| \end{cases} \end{aligned}$$

Proof.

$$\begin{aligned} & \Pr\left(\sup_{0 \leq s \leq \Delta} |X_s - X_0| \geq a \mid X_\Delta = x_\Delta\right) \\ & \leq \Pr\left(\sup_{0 \leq s \leq \Delta} X_s - X_0 \geq a \mid X_\Delta = x_\Delta\right) + \Pr\left(\inf_{0 \leq s \leq \Delta} X_s - X_0 \leq -a \mid X_\Delta = x_\Delta\right) \\ & = \begin{cases} \exp\left\{-\frac{2a}{\Delta}[a - (x_\Delta - x_0)]\right\} + \exp\left\{-\frac{2a}{\Delta}[a + (x_\Delta - x_0)]\right\} & a > |x_\Delta - x_0| \\ 1, & a \leq |x_\Delta - x_0| \end{cases} \\ & \leq \begin{cases} 2 \exp\left\{-\frac{2a}{\Delta}[a - |x_\Delta - x_0|]\right\} & a > |x_\Delta - x_0| \\ 1, & a \leq |x_\Delta - x_0| \end{cases} \end{aligned}$$

\square

Proof of Lemma 1.

Proof.

$$\begin{aligned}
& \Pr(E_1 > 0 \mid \kappa = k > 0) \\
&= \mathbb{E} \left\{ \mathbb{I} \left[\left(\prod_{j=1}^k \left(1 + \frac{\Delta}{\eta} (\lambda(X_0) - \lambda(X_{\tau_j})) \right) \right) > 0 \right] \mid \kappa = k, \tau_1, \dots, \tau_k \right\} \\
&\geq \mathbb{E} \left\{ \mathbb{I} \left[\max_{j \in \{1, \dots, k\}} \frac{\Delta}{\eta} |\lambda(X_0) - \lambda(X_{\tau_j})| < 1 \right] \mid \kappa = k, \tau_1, \dots, \tau_k \right\} \\
&= \Pr \left(\max_{j \in \{1, \dots, k\}} |\lambda(X_0) - \lambda(X_{\tau_j})| \leq \frac{\eta}{\Delta} \mid \kappa = k, \tau_1, \dots, \tau_k \right).
\end{aligned}$$

We can obtain an upperbound for $\Pr(E_1 < 0 \mid \kappa = k)$ by

$$\begin{aligned}
\Pr(E_1 < 0 \mid \kappa = k) &\leq \Pr \left(\max_{j \in \{1, \dots, k\}} |\lambda(X_0) - \lambda(X_{\tau_j})| \geq \frac{\eta}{\Delta} \mid \kappa = k, \tau_1, \dots, \tau_k \right) \\
&\leq \Pr \left(\max_{j \in \{1, \dots, k\}} |X_0 - X_{\tau_j}| \geq \frac{\eta}{\Delta l} \mid \kappa = k, \tau_1, \dots, \tau_k \right)
\end{aligned}$$

where we assume $\lambda(\cdot)$ is an l -Lipschitz function.

$$\Pr \left(\max_{j \in \{1, \dots, k\}} |X_0 - X_{\tau_j}| \geq \frac{\eta}{\Delta l} \mid \kappa = k, \tau_1, \dots, \tau_k \right) \leq \Pr \left(\sup_{0 \leq s \leq \Delta} |X_0 - X_s| \geq \frac{\eta}{\Delta l} \right).$$

Applying Proposition 5, we have

$$\Pr(E_1 < 0 \mid \kappa > 0) \leq \begin{cases} 2 \exp \left\{ -\frac{2\eta}{\Delta l} \left(\frac{\eta}{\Delta l} - |x_\Delta - x_0| \right) \right\}, & \frac{\eta}{\Delta l} \geq |x_\Delta - x_0| \\ 1, & \frac{\eta}{\Delta l} \leq |x_\Delta - x_0| \end{cases}$$

□

APPENDIX C. EXPECTATION OF THE PROBABILITY BOUND

This section establishes the unqualified bound ((13)). The goal is to determine the following expectation for $Y = |X_\Delta - X_0|$ where $X_\Delta - X_0 \sim \mathcal{N}(0, \Delta)$, (thus Y is a half-normal random variable):

$$\begin{aligned}
 & \mathbb{E} \{ \mathbb{I} [E < 0] | \kappa > 0 \} \\
 &= \mathbb{E} \left\{ \mathbb{I} [E < 0] \times \mathbb{I} \left[Y < \frac{\eta}{\Delta l} \right] + \mathbb{I} [E < 0] \times \mathbb{I} \left[Y \geq \frac{\eta}{\Delta l} \right] | \kappa > 0 \right\} \\
 &\leq \mathbb{E} \left\{ 2 \exp \left(-\frac{2\eta}{\Delta l} \left(\frac{\eta}{\Delta l} - Y \right) \right) \mathbb{I} \left[Y < \frac{\eta}{\Delta l} \right] \right\} + \Pr \left(Y \geq \frac{\eta}{\Delta l} \right) \\
 &= \int_0^\infty 2 \exp \left(-\frac{2\eta}{\Delta l} \left(\frac{\eta}{\Delta l} - y \right) \right) \mathbb{I} \left[y < \frac{\eta}{\Delta l} \right] \times \frac{\sqrt{2}}{\sqrt{\pi\Delta}} \exp \left(-\frac{y^2}{2\Delta} \right) dy + \Pr \left(Y \geq \frac{\eta}{\Delta l} \right) \\
 &= \int_0^{\frac{\eta}{\Delta l}} \frac{2\sqrt{2}}{\sqrt{\pi\Delta}} \exp \left(-\frac{2\eta^2}{\Delta^3 l^2} \right) \times \exp \left(-\frac{(y - \frac{2\eta}{\Delta l})^2 - \frac{4\eta^2}{\Delta^2 l^2}}{2\Delta} \right) dy + \Pr \left(Y \geq \frac{\eta}{\Delta l} \right) \\
 &= \int_0^{\frac{\eta}{\Delta l}} \frac{2\sqrt{2}}{\sqrt{\pi\Delta}} \exp \left(-\frac{(y - \frac{2\eta}{\Delta l})^2}{2\Delta} \right) dy + \Pr \left(|X_\Delta - X_0| \geq \frac{\eta}{\Delta l} \right) \\
 &= 4 \left[\Phi \left(\frac{2\eta}{\Delta^{\frac{3}{2}} l} \right) - \Phi \left(\frac{\eta}{\Delta^{\frac{3}{2}} l} \right) \right] + 2 \times \left(1 - \Phi \left(\frac{\eta}{\Delta^{\frac{3}{2}} l} \right) \right) \\
 &= 2 + 4\Phi \left(\frac{2\eta}{\Delta^{\frac{3}{2}} l} \right) - 6\Phi \left(\frac{\eta}{\Delta^{\frac{3}{2}} l} \right).
 \end{aligned}$$

APPENDIX D. PROOF OF LEMMA 2

Proof.

$$\begin{aligned}
 E_i &= \exp(-\Delta\lambda(X_{(i-1)\Delta})) \prod_{j=1}^{\kappa_i} \left(1 + \frac{\lambda(X_{(i-1)\Delta}) - \lambda(X_{\tau_j})}{l} \right) \\
 &\leq \prod_{j=1}^{\kappa_i} (1 + |X_{(i-1)\Delta} - X_{\tau_j}|) \\
 &\leq \prod_{j=1}^{\kappa_i} \left(1 + \max_{(i-1)\Delta \leq s \leq i\Delta} |X_s - X_{(i-1)\Delta}| \right) \\
 (25) \quad &= \left(1 + \max_{0 \leq s \leq \Delta} |B_s| \right)^{\kappa_i} =: F_i.
 \end{aligned}$$

We truncate the Poisson estimate as $E_i^+ = E_i \mathbb{I}_{A_i^c}$ and bound $\mathbb{I}_A \prod_{i=1}^m E_i$ as follows.

$$(26) \quad \left| \mathbb{E} \left\{ \mathbb{I}_A \prod_{i=1}^m E_i \right\} \right| \leq \mathbb{E} \left\{ \prod_{i=1}^m E_i^2 \right\}^{\frac{1}{2}} \mathbb{E} \{ \mathbb{I}_A \}^{\frac{1}{2}}.$$

The term $\mathbb{E} \{ \mathbb{I}_A \}^{\frac{1}{2}}$ can be bound using the union bound

$$(27) \quad \mathbb{E} \{ \mathbb{I}_A \} \leq \sum_{i=1}^m \mathbb{E} \{ \mathbb{I}_{A_i} \} = m \mathbb{E} \{ \mathbb{I}_{A_1} \} = m \times 2 \exp \left(-\frac{1}{2\Delta} \right)$$

The other term can be proved to be finite, i.e. $\mathbb{E} \left\{ \prod_{i=1}^m E_i^2 \right\} < \infty$. Since the increment of Brownian motion X is independent of each other, and using the inequality (25), one can show

$$\mathbb{E} \left\{ \prod_{i=1}^m E_i^2 \right\} \leq \mathbb{E} \left\{ \prod_{i=1}^m F_i^2 \right\} = \mathbb{E} \{ F_i^2 \}^m, \quad \forall i.$$

It remains therefore to bound $\mathbb{E} \{ F_i^2 \}$.

$$\begin{aligned} \mathbb{E} \{ F_i^2 \} &= \mathbb{E} \left\{ \left(1 + \max_{0 \leq s \leq \Delta} |B_s| \right)^{2\kappa_i} \right\} \\ &= \mathbb{E} \left\{ \sum_{k=0}^{\infty} \frac{(\Delta l)^k e^{-\Delta l}}{k!} \left(1 + \max_{0 \leq s \leq \Delta} |B_s| \right)^{2k} \right\} \\ &= \exp(-\Delta l) \mathbb{E} \left\{ \exp \left(\Delta l \left(1 + \max_{0 \leq s \leq \Delta} |B_s| \right)^2 \right) \right\} \\ &\leq \exp(-\Delta l) \mathbb{E} \left\{ \exp \left(\Delta l \left(2 + 2 \times \max_{0 \leq s \leq \Delta} B_s^2 \right) \right) \right\} \\ &= \exp(\Delta l) \mathbb{E} \left\{ \exp \left(2\Delta l \times \max_{0 \leq s \leq \Delta} B_s^2 \right) \right\} \\ &= \exp(\Delta l) \times \int_0^{\infty} \Pr \left(\exp \left(2\Delta l \times \max_{0 \leq s \leq \Delta} B_s^2 \right) > w \right) dw \\ &= \exp(\Delta l) \times \left[1 + \int_1^{\infty} \Pr \left(\exp \left(2\Delta l \times \max_{0 \leq s \leq \Delta} B_s^2 \right) > w \right) dw \right] \\ &= \exp(\Delta l) \times \left[1 + \int_1^{\infty} \Pr \left(\max_{0 \leq s \leq \Delta} |B_s| > \sqrt{\frac{\log(w)}{2\Delta l}} \right) dw \right] \\ &\leq \exp(\Delta l) \times \left[1 + \int_1^{\infty} 2 \exp \left(-\frac{\log(w)}{4\Delta^2 l} \right) dw \right] \\ &= \exp(\Delta l) \times \left[1 + \int_1^{\infty} 2w^{-\frac{1}{4\Delta^2 l}} dw \right] \\ &= \exp(\Delta l) \times \left(\frac{1 + 4\Delta^2 l}{1 - 4\Delta^2 l} \right) \end{aligned}$$

where in the fourth last line we apply the inequality for running maximum of Brownian motion which starts at zero, i.e. $\Pr(\max_{0 \leq s \leq \Delta} |B_s| > a) \leq 2 \exp\left(-\frac{a^2}{2\Delta}\right)$ for any positive number a .

Therefore,

$$(28) \quad \mathbb{E} \{ E_1^2 \cdots E_m^2 \} \leq \exp(Tl) \times \left(\frac{1 + 4\Delta^2 l}{1 - 4\Delta^2 l} \right)^m.$$

Plugging (27) and (28) into (26) concludes the proof. \square

APPENDIX E. WALD EXPERIMENTS

In this section, we wish to numerically show that the Wald estimate is biased, i.e. $\mathbb{E}^\theta(\hat{L}(\theta))/L(\theta)$ changes as θ changes where $K = \inf\{k > 0 : E^{(1)} + \dots + E^{(k)} > 0\}$, $\hat{L}(\theta) = \sum_{i=1}^K E^{(i)}$ and $L(\theta) = \mathbb{E}^\theta(G^\theta(X_0))$.

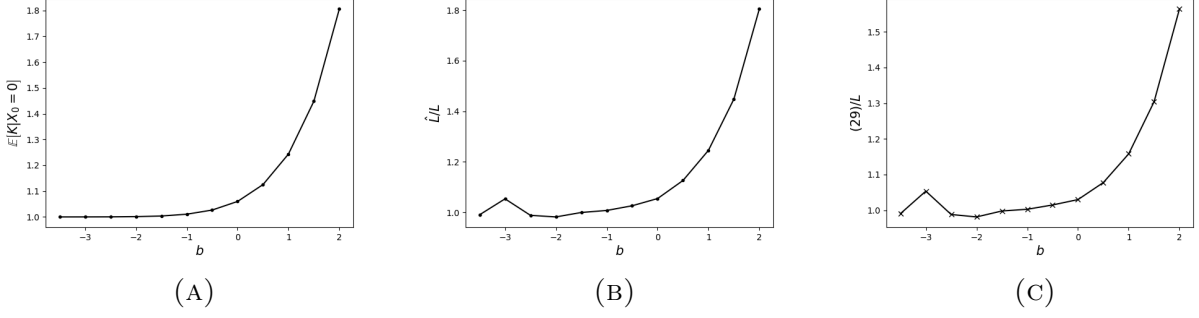


FIGURE 12. (a) Plot of $\mathbb{E}^\theta(K|X_0 = 0)$, (b) \hat{L}'/L and (c) estimate (29)/ L versus $\theta = b$.

Here is an example of which we know the true solution to. The dynamics that describes how one dimensional process X evolves is given by

$$dX_t = bdt + dW_t$$

where b is some constant and W is a one dimensional Brownian motion. Hence

$$X_t|X_{t'} = x \sim \mathcal{N}(x + b \times (t - t'), t - t').$$

Thus, $\theta = b$ in this case. We can exactly calculate $L(\theta)$ for $\lambda(x) = x + 10$,

$$L(\theta) = \mathbb{E} \left(\exp \left(- \int_0^T \lambda(X_t) dt \right) \middle| X_0 = 0 \right) = \exp \left(-10T - \frac{b}{2}T^2 + \frac{1}{6}T^3 \right)$$

where the expectation is taken with respect to Brownian motion $X|X_0 = 0$. Note that $\int_0^T (10 + X_0 + bt + W_t - W_0) dt \sim \mathcal{N} \left(10T + \frac{b}{2}T^2, \frac{1}{3}T^3 \right)$ for $X_0 = W_0 = 0$.

We obtain $N = 10^6$ independent samples $\hat{L}(b)$ for every value of b :

$$\hat{L}'(b) = \frac{1}{N} \sum_{j=1}^N \sum_{i=1}^{K_j} E_j^{(i)} \approx \mathbb{E}^\theta(\hat{L}(b))$$

where $K_j = \inf\{k > 0 : E_j^{(1)} + \dots + E_j^{(k)} > 0\}$. Each $E_j^{(i)}$ is an independent sample where $E_j^{(i)} \leftarrow \text{PE}(T, 0, T, 0)$. Figure 12a shows that as b increases, the number of draws to make Wald estimate positive increases. For this example E is

$$E = \exp(-T(X_0 + 10)) \prod_{i=1}^{\kappa} [1 + [X_0 - X_{\tau_i}]]$$

where $\kappa \sim \mathcal{P}o(T)$ and $\tau_1, \dots, \tau_\kappa \sim \mathcal{U}(0, T)$ are i.i.d. samples. Larger b (i.e. larger drift dragging the particle towards positive direction) increases the chances of meeting negative Poisson estimate. In Figure 12b, we notice a clear trend that the empirical ratio, $\hat{L}'(b)/L(b)$, increases with b . Finally we plot

$$(29) \quad \frac{1}{N} \sum_{j=1}^N \frac{1}{K_j} \sum_{i=1}^{K_j} E_j^{(i)}.$$

APPENDIX F. EXACT COMPUTATION OF LIKELIHOOD FUNCTION

This section is to determine the following likelihood function.

$$\mathbb{E} \left\{ \exp \left[- \int_{\tau}^T (\alpha X_t + \beta) dt \right] \middle| X_{\tau} = x_0, X_T = x_1 \right\}$$

The procedure can be splitted into 4 steps.

- (1) As $X_t|X_T$ is a Gaussian process, the Lebesgue integral is Gaussian random variable, see [14]: approximate the given integral as Riemann sums and each Riemann sum is Gaussian and hence the limit will also be Gaussian.

$$\left(\int_{\tau}^T \alpha X_t + \beta dt \middle| X_{\tau} = x_0, X_T = x_1 \right) \sim \mathcal{N}(\alpha\mu + \beta(T - \tau), \alpha^2\sigma^2)$$

- (2) Calculate mean μ :

$$\begin{aligned} \mathbb{E} \left[\int_{\tau}^T X_t dt \middle| X_{\tau} = x_0, X_T = x_1 \right] &= \int_{\tau}^T \mathbb{E} [X_t | X_{\tau} = x_0, X_T = x_1] dt \\ &= \int_{\tau}^T x_0 + \frac{t - \tau}{T - \tau} (x_1 - x_0) dt \\ &= \frac{1}{2} (T - \tau) (x_0 + x_1) \end{aligned}$$

- (3) Calculate variance σ^2 :

$$\begin{aligned} &\mathbb{E} \left[\left(\int_{\tau}^T X_t dt \right) \left(\int_{\tau}^T X_t dt \right) \middle| X_{\tau} = x_0, X_T = x_1 \right] - \mu^2 \\ &= \mathbb{E} \left[\int_{[\tau, T]^2} X_u X_v dudv \middle| X_{\tau} = x_0, X_T = x_1 \right] - \mu^2 \\ &= \int_{[\tau, T]^2} \mathbb{E} [X_u X_v | X_{\tau} = x_0, X_T = x_1] dudv - \mu^2 \\ &= \int_{[\tau, T]^2} \text{cov}(X_u, X_v) + \mathbb{E} [X_u | X_{\tau} = x_0, X_T = x_1] \times \mathbb{E} [X_v | X_{\tau} = x_0, X_T = x_1] dudv - \mu^2 \\ &= \int_{[\tau, T]^2} \frac{(u \wedge v - \tau)(T - u \vee v)}{T - \tau} + \left(x_0 + \frac{u - \tau}{T - \tau} (x_1 - x_0) \right) \times \left(x_0 + \frac{v - \tau}{T - \tau} (x_1 - x_0) \right) dudv - \mu^2 \\ &= \int_{\tau}^T \int_{\tau}^v \frac{(u - \tau)(T - v)}{T - \tau} dudv + \int_{\tau}^T \int_v^T \frac{(v - \tau)(T - u)}{T - \tau} dudv \\ &= \frac{(T - \tau)^3}{12} \end{aligned}$$

- (4) Calculate the likelihood:

$$\begin{aligned} &\mathbb{E} \left\{ \exp \left[- \int_{\tau}^T (\alpha X_t + \beta) dt \right] \middle| X_{\tau} = x_0, X_T = x_1 \right\} \\ &= \exp \left[- \frac{\alpha}{2} (T - \tau) (x_0 + x_1) - \beta(T - \tau) + \frac{\alpha^2 (T - \tau)^3}{24} \right] \end{aligned}$$

Therefore, the exact likelihood for $t_{1:n_p}$ and $y_{t_1:t_{n_p}}$, where n_p is the number of observations, is

$$\mathcal{L} = \mathbb{E} \left\{ \left[\prod_{i=1}^{n_p} (X_{t_i} + 10) g^\theta(y_{t_i} | X_{t_i}) \times \exp \left(-\frac{t_i - t_{i-1}}{2} (X_{t_{i-1}} + X_{t_i}) - 10(t_i - t_{i-1}) + \frac{(t_i - t_{i-1})^3}{24} \right) \right] \right. \\ \left. \times \exp \left(-\frac{T - t_{n_p}}{2} (X_{t_{n_p}} + X_T) - 10(T - t_{n_p}) + \frac{(T - t_{n_p})^3}{24} \right) \right\}.$$

To find the ground truth for values of $n_p > 2$, we use Algorithm 3 with line 8 using the exact evaluation (given by (30)). This allows the computation of Monte Carlo estimate described in Section 5.1.

$$(30) \quad E_k^{(i)} = \exp \left[-\frac{1}{2} (t_k^\Delta - t_{k-1}^\Delta) (X_{k-1}^\Delta + X_k^\Delta) - 10 (t_k^\Delta - t_{k-1}^\Delta) + \frac{(t_k^\Delta - t_{k-1}^\Delta)^3}{24} \right].$$

APPENDIX G. NO OBSERVATION CASE AND TWO OBSERVATION CASE

The exact likelihood for no observation received within $[0, T]$ is

$$\begin{aligned} & \mathbb{E} \left\{ \exp \left(-\int_0^T \lambda(X_s) ds \right) \right\} \\ &= \mathbb{E} \left\{ \mathbb{E} \left[\exp \left(-\int_0^T \lambda(X_s) ds \right) \mid X_0 = 0, X_T \right] \right\} \\ &= \mathbb{E} \left\{ \exp \left(-\frac{TX_T}{2} - 10T + \frac{T^3}{24} \right) \right\} \\ &= \int_{-\infty}^{\infty} \frac{1}{\sqrt{2\pi T}} \exp \left(-10T + \frac{T^3}{24} + \frac{T^3}{8} \right) \exp \left(-\frac{(x_T - \frac{T^2}{2})^2}{2T} \right) dx_T \\ &= \exp \left(-10T + \frac{T^3}{6} \right) \end{aligned}$$

and the exact likelihood for two observations received within $[0, T]$ is

$$\begin{aligned} \mathcal{L} &= \mathbb{E} \left\{ \left[\prod_{i=1}^2 \lambda(X_{t_i}) g^\theta(y_{t_i} | X_{t_i}) \exp \left(-\int_{t_{i-1}}^{t_i} \lambda(X_s) ds \right) \right] \exp \left(-\int_{t_2}^T \lambda(X_s) ds \right) \right\} \\ &= \int_{-\infty}^{\infty} \int_{-\infty}^{\infty} \int_{-\infty}^{\infty} (v_1 + 10) (v_1 + v_2 + 10) \times \frac{1}{2\pi\sigma_y^2} \exp \left(-\frac{(y_{t_1} - v_1)^2 + (y_{t_2} - v_1 - v_2)^2}{2\sigma_y^2} \right) \\ &\quad \times \exp \left(-\frac{t_1 v_1}{2} - \frac{t_2 - t_1}{2} (2v_1 + v_2) - \frac{T - t_2}{2} (2v_1 + 2v_2 + v_3) - 10T \right) \\ &\quad \times \exp \left(\frac{t_1^3 + (t_2 - t_1)^3 + (T - t_2)^3}{24} \right) \times \frac{1}{\sqrt{2\pi t_1}} \times \frac{1}{\sqrt{2\pi(t_2 - t_1)}} \times \frac{1}{\sqrt{2\pi(T - t_2)}} \\ &\quad \times \exp \left(-\frac{v_1^2}{2t_1} - \frac{v_2^2}{2(t_2 - t_1)} - \frac{v_3^2}{2(T - t_2)} \right) dv_3 dv_2 dv_1 \end{aligned}$$

The first integral with respect to v_3 is

$$\int_{-\infty}^{\infty} \exp \left(-\frac{T - t_2}{2} v_3 - \frac{v_3^2}{2(T - t_2)} \right) dv_3 = \sqrt{2\pi(T - t_2)} \exp \left(\frac{1}{8} (T - t_2)^3 \right).$$

The second integral with respect to v_2 is

$$\begin{aligned}
& \int_{-\infty}^{\infty} (v_1 + v_2 + 10) \exp\left(-\frac{(y_{t_2} - v_1 - v_2)^2}{2\sigma_y^2}\right) \\
& \times \exp\left(-\frac{t_2 - t_1}{2}v_2 - \frac{T - t_2}{2} \times 2v_2\right) \times \exp\left(-\frac{v_2^2}{2(t_2 - t_1)}\right) dv_2 \\
& = \int_{-\infty}^{\infty} (v_1 + v_2 + 10) \exp\left(-\left(\frac{1}{2\sigma_y^2} + \frac{1}{2(t_2 - t_1)}\right)v_2^2 - \left(\frac{-y_{t_2} + v_1}{\sigma_y^2} - \frac{t_1 + t_2 - 2T}{2}\right)v_2\right) \\
& \times \exp\left(-\frac{y_{t_2}^2 - 2v_1y_{t_2} + v_1^2}{2\sigma_y^2}\right) dv_2 \\
& = \int_{-\infty}^{\infty} (v_1 + v_2 + 10) \exp\left(-\frac{y_{t_2}^2 - 2v_1y_{t_2} + v_1^2}{2\sigma_y^2} + \frac{\mu_2^2}{2\sigma_2^2}\right) \exp\left(-\frac{(v_2 - \mu_2)^2}{2\sigma_2^2}\right) dv_2 \\
& = \sqrt{2\pi\sigma_2^2} (\mu_2 + v_1 + 10) \exp\left(-\frac{y_{t_2}^2 - 2v_1y_{t_2} + v_1^2}{2\sigma_y^2} + \frac{\mu_2^2}{2\sigma_2^2}\right)
\end{aligned}$$

where

$$\sigma_2^2 = \left(\frac{1}{\sigma_y^2} + \frac{1}{t_2 - t_1}\right)^{-1}, \quad \mu_2 = \sigma_2^2 \left(\frac{y_{t_2} - v_1}{\sigma_y^2} + \frac{t_1 + t_2 - 2T}{2}\right) = \sigma_2^2(av_1 + b)$$

and for

$$a = -\frac{1}{\sigma_y^2}, \quad b = \frac{y_{t_2}}{\sigma_y^2} + \frac{t_1 + t_2 - 2T}{2}.$$

The third integral with respect to v_1 is as follows,

$$\begin{aligned}
& \int_{-\infty}^{\infty} (v_1 + 10) (\mu_2 + v_1 + 10) \exp\left(-\frac{(y_{t_1} - v_1)^2 + y_{t_2}^2 - 2v_1y_{t_2} + v_1^2}{2\sigma_y^2}\right) \\
& \times \exp\left(\frac{\sigma_2^2}{2}(a^2v_1^2 + 2abv_1 + b^2)\right) \times \exp\left(-\frac{t_1v_1}{2} - (t_2 - t_1)v_1 - (T - t_2)v_1\right) \exp\left(-\frac{v_1^2}{2t_1}\right) dv_1 \\
& = \int_{-\infty}^{\infty} [(\sigma_2^2a + 1)v_1^2 + (10(\sigma_2^2a + 1) + \sigma_2^2b + 20)v_1 + 10\sigma_2^2b + 100] \\
& \times \exp\left(-\left(\frac{1}{\sigma_y^2} - \frac{a^2\sigma_2^2}{2} + \frac{1}{2t_1}\right)v_1^2 + \left(\frac{2y_{t_1} + 2y_{t_2}}{2\sigma_y^2} + ab\sigma_2^2 + \frac{t_1 - 2T}{2}\right)v_1\right) \\
& \times \exp\left(-\frac{y_{t_1}^2 + y_{t_2}^2}{2\sigma_y^2} + \frac{b^2\sigma_2^2}{2}\right) dv_1 \\
& = \sqrt{2\pi\sigma_1^2} [(\sigma_2^2a + 1)(\mu_1^2 + \sigma_1^2) + (10(\sigma_2^2a + 1) + \sigma_2^2b + 20)\mu_1 + 10\sigma_2^2b + 100] \\
& \times \exp\left(-\frac{y_{t_1}^2 + y_{t_2}^2}{2\sigma_y^2} + \frac{b^2\sigma_2^2}{2} + \frac{\mu_1^2}{2\sigma_1^2}\right)
\end{aligned}$$

where $\sigma_1^2 = \left(\frac{2}{\sigma_y^2} - a^2\sigma_2^2 + \frac{1}{t_1}\right)^{-1}$ and $\mu_1 = \sigma_1^2 \left(\frac{y_{t_1} + y_{t_2}}{\sigma_y^2} + ab\sigma_2^2 + \frac{t_1 - 2T}{2}\right)$

Therefore,

$$\begin{aligned}
\mathcal{L} & = \frac{1}{2\pi\sigma_y^2} \times \frac{\sigma_1\sigma_2}{\sqrt{t_1(t_2 - t_1)}} [(\sigma_2^2a + 1)(\mu_1^2 + \sigma_1^2) + (10(\sigma_2^2a + 1) + \sigma_2^2b + 20)\mu_1 + 10\sigma_2^2b + 100] \\
& \times \exp\left(-\frac{y_{t_1}^2 + y_{t_2}^2}{2\sigma_y^2} + \frac{b^2\sigma_2^2}{2} + \frac{\mu_1^2}{2\sigma_1^2}\right) \times \exp\left(-10T + \frac{t_1^3 + (t_2 - t_1)^3 + (T - t_2)^3}{24} + \frac{1}{8}(T - t_2)^3\right).
\end{aligned}$$

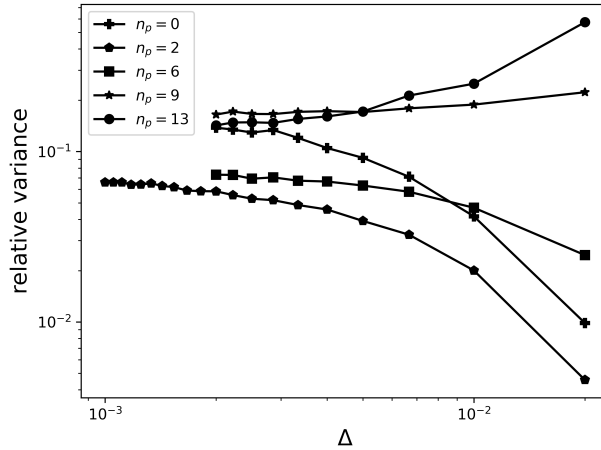


FIGURE 13. Plot of relative variance versus Δ for different values of n_p and fixed $N = 100$ in log scale.

The exact likelihood are used to compute the relative MSE for Section 5 and Appendix H.

APPENDIX H. EMPIRICAL RELATIONSHIP BETWEEN RELATIVE VARIANCE AND Δ

Figure 13 reports the relationship between relative variance and Δ for different n_p values and fixed $N = 100$. For $n_p = 0$ and $n_p = 2$ cases, the exact likelihood is computed using solutions calculated in Section G, for other larger values of n_p , the Monte Carlo estimate \mathcal{L}_{MC} is used in relative variance computation. Results show that the relationship between relative variance and Δ can be highly n_p -dependent. As n_p of problem increases, the rate of change in relative variance becomes less positive when Δ approaches zero. A more general trend that applies to all values of n_p is that the relative variance eventually becomes constant as Δ goes to zero.

APPENDIX I. THINNING ALGORITHM FOR CREATING DATA

This section describes the thinning algorithm we use to generate observation data. Please refer Algorithm 4 for details.

APPENDIX J. ADDITIONAL EXPERIMENTS

In Figure 9a, we plot the true trajectory of a molecule, and simulate using parameters $\{\theta = (1.0, 1.0, 1.0)^\top, \mu = (0.5, 0.5, 6.0)^\top, p_0 = 0.01\}$ for time interval $[0, 5.0]$. Other parameters remain the same as in Section 5.2. Figure 9c shows the filtered (x_1, x_2) mean locations of molecules, which deviate from their right positions. Figure 9d shows the filtered mean of x_3 and regions of ± 1 standard deviation together with the true state of X_3 at the observation times. In comparison to the Figure 9c and 9d, Figure 14c and 14d shows that higher values of x_3 degrade the estimation quality of particle filtering algorithm on the state of molecule and this is due to the exponential function structure of Born and Wolf image function which generates photons that are detected very far from the true molecule position.

REFERENCES

- [1] Andrieu, C., A. Doucet, and R. Holenstein (2010). Particle Markov chain Monte Carlo methods. *Journal of the Royal Statistical Society: Series B (Statistical Methodology)* 72(3), 269–342.
- [2] Axelrod, D. (2001). Total internal reflection fluorescence microscopy in cell biology. *Traffic* 2(11), 764–774.

Algorithm 4: Thinning Algorithm for simulating the observation times with intensity function $\lambda(X_t)$ on $[0, T]$

Input: $\lambda_{\max} = \lambda_0, T$

- 1 Generate $N \sim \mathcal{P}o(\lambda_{\max}T)$;
- 2 Generate $t_1, t_2, \dots, t_N \sim \mathcal{U}(0, T)$;
- 3 Sort t_1, t_2, \dots, t_N and relabel them so that $t_1 < t_2 < \dots < t_N$;
- 4 Generate $X_0 \sim \nu(x)$ and set $\tau = 0$;
- 5 **for** $i \in \{1 : N\}$ **do**
- 6 Propagate X_{t_i} from previous τ , i.e. $X_{t_i} \sim f_{t_i-\tau}^\theta(x_{t_i}|X_\tau)$;
- 7 Generate $U \sim \mathcal{U}(0, 1)$;
- 8 **if** $U \leq \lambda(X_{t_i})/\lambda_{\max}$ **then**
- 9 Keep t_i as a real observation time and set $\tau = t_i$;
- 10 Generate y_{t_i} which is a realisation of $Y_{t_i} \sim g^\theta(y|X_{t_i})$ with Born and Wolf point spread function.

Output: all pairs of (t_i, y_{t_i})

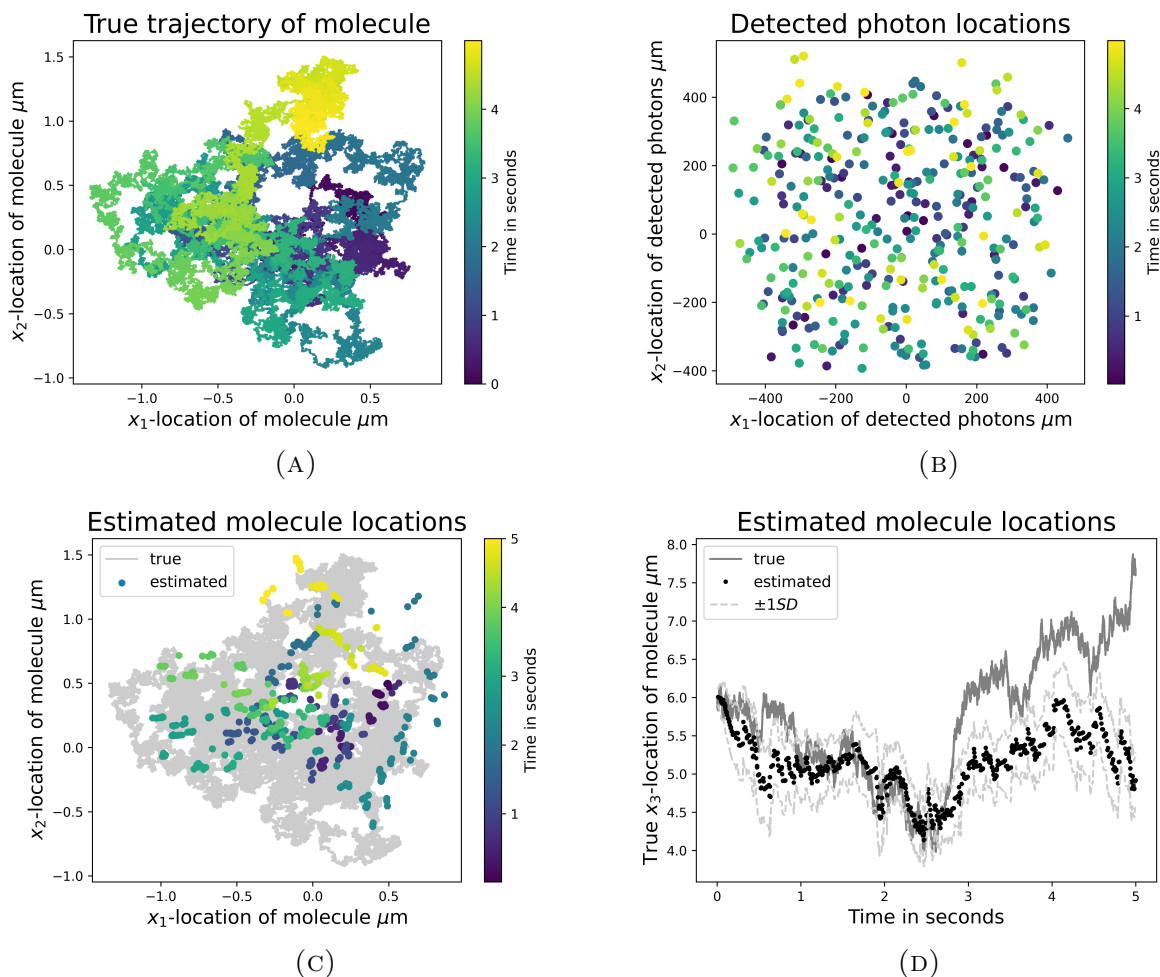


FIGURE 14. (a) True trajectory of a molecule; (b) observed photon locations; (c) estimated (x_1, x_2) molecule locations and (d) true x_3 molecule locations and estimated location.

- [3] Beskos, A., O. Papaspiliopoulos, G. O. Roberts, and P. Fearnhead (2006). Exact and computationally efficient likelihood-based estimation for discretely observed diffusion processes (with discussion). *Journal of the Royal Statistical Society: Series B (Statistical Methodology)* 68(3), 333–382.
- [4] Black, F. and M. Scholes (2019). The pricing of options and corporate liabilities. In *World Scientific Reference on Contingent Claims Analysis in Corporate Finance: Volume 1: Foundations of CCA and Equity Valuation*, pp. 3–21. World Scientific.
- [5] Blanchet, J. and K. Murthy (2018). Exact simulation of multidimensional reflected brownian motion. *Journal of Applied Probability* 55(1), 137–156.
- [6] Born, M. and E. Wolf (2013). *Principles of optics: electromagnetic theory of propagation, interference and diffraction of light*. Elsevier.
- [7] Chopin, N., S. S. Singh, T. Soto, and M. Vihola (2022). On resampling schemes for particle filters with weakly informative observations. *arXiv preprint arXiv:2203.10037*.
- [8] d’Avigneau, A. M., S. S. Singh, and R. J. Ober (2022). Limits of accuracy for parameter estimation and localization in single-molecule microscopy via sequential Monte Carlo methods. *SIAM Journal on Imaging Sciences* 15(1), 139–171.
- [9] Del Moral, P. (2004). *Feynman-Kac formulae: genealogical and interacting particle systems with applications*, Volume 88. Springer.
- [10] Durham, G. B. and A. R. Gallant (2002). Numerical techniques for maximum likelihood estimation of continuous-time diffusion processes. *Journal of Business & Economic Statistics* 20(3), 297–338.
- [11] Evans, L. C. (2012). *An introduction to stochastic differential equations*, Volume 82. American Mathematical Soc.
- [12] Fearnhead, P., O. Papaspiliopoulos, and G. O. Roberts (2008). Particle filters for partially observed diffusions. *Journal of the Royal Statistical Society: Series B (Statistical Methodology)* 70(4), 755–777.
- [13] Fearnhead, P., O. Papaspiliopoulos, G. O. Roberts, and A. Stuart (2010). Random-weight particle filtering of continuous time processes. *Journal of the Royal Statistical Society: Series B (Statistical Methodology)* 72(4), 497–512.
- [14] Folland, G. B. (1999). *Real analysis: modern techniques and their applications*, Volume 40. John Wiley & Sons.
- [15] Gillespie, D. T. (1976). A general method for numerically simulating the stochastic time evolution of coupled chemical reactions. *Journal of computational physics* 22(4), 403–434.
- [16] Gillespie, D. T. (1977). Exact stochastic simulation of coupled chemical reactions. *The journal of physical chemistry* 81(25), 2340–2361.
- [17] Haario, H., E. Saksman, and J. Tamminen (2001). An adaptive Metropolis algorithm. *Bernoulli*, 223–242.
- [18] Jasra, A., F. Yu, and J. Heng (2020). Multilevel particle filters for the non-linear filtering problem in continuous time. *Statistics and Computing* 30(5), 1381–1402.
- [19] Jazwinski, A. H. (2007). *Stochastic processes and filtering theory*. Courier Corporation.
- [20] Kloeden, P. and E. Platen (2011). *Numerical Solution of Stochastic Differential Equations*. Stochastic Modelling and Applied Probability. Springer Berlin Heidelberg.
- [21] McAdams, H. H. and A. Arkin (1997). Stochastic mechanisms in gene expression. *Proceedings of the National Academy of Sciences* 94(3), 814–819.
- [22] Merton, R. C. (1975). Optimum consumption and portfolio rules in a continuous-time model. In *Stochastic optimization models in finance*, pp. 621–661. Elsevier.
- [23] Mörters, P. and Y. Peres (2010). *Brownian motion*, Volume 30. Cambridge University Press.
- [24] Nicolau, J. (2002). A new technique for simulating the likelihood of stochastic differential equations. *The Econometrics Journal* 5(1), 91–103.
- [25] Ober, R. J., E. S. Ward, and J. Chao (2020). *Quantitative Bioimaging: An Introduction to Biology, Instrumentation, Experiments, and Data Analysis for Scientists and Engineers*. CRC Press.

- [26] Obukhov, A. M. (1959). Description of turbulence in terms of lagrangian variables. *Advances in Geophysics* 6, 113–116.
- [27] Papaspiliopoulos, O. (2011). *Monte Carlo probabilistic inference for diffusion processes: a methodological framework*, pp. 82–103. Cambridge University Press.
- [28] Pardoux, E. and M. Pignol (1984). Etude de la stabilité de la solution d’une eds bilinéaire à coefficients périodiques. application au mouvement des pales d’hélicoptère. In *Analysis and Optimization of systems*, pp. 92–103. Springer.
- [29] Rousset, M. and A. Doucet (2006). Discussion on ‘exact and computationally efficient likelihood-based inference for discretely observed diffusion processes’. *Journal of the Royal Statistical Society: Series B (Statistical Methodology)* 68(3), 375–376.
- [30] Szalai, A. M., B. Siarry, J. Lukin, D. J. Williamson, N. Unsain, A. Cáceres, M. Pilo-Pais, G. Acuna, D. Refojo, D. M. Owen, et al. (2021). Three-dimensional total-internal reflection fluorescence nanoscopy with nanometric axial resolution by photometric localization of single molecules. *Nature communications* 12(1), 1–13.
- [31] Vahid, M. R., B. Hanzon, and R. J. Ober (2020). Fisher information matrix for single molecules with stochastic trajectories. *SIAM Journal on Imaging Sciences* 13(1), 234–264.
- [32] Wagner, W. (1988). Unbiased multi-step estimators for the Monte Carlo evaluation of certain functional integrals. *Journal of computational physics* 79(2), 336–352.
- [33] Wagner, W. (1989). Undiased Monte Carlo estimators for functionals of weak solutions of stochastic diffretial equations. *Stochastics: An International Journal of Probability and Stochastic Processes* 28(1), 1–20.
- [34] Yonekura, S. and A. Beskos (2022). Online smoothing for diffusion processes observed with noise. *Journal of Computational and Graphical Statistics* (just-accepted), 1–35.